REPORT DOCUMENTATION PAGE

AFRL-SR-BL-TR-98-0204

Form Approved OMB No. 0704-0188

1. AGENCY USE ONLY (Leave blank)	2. REPORT DATE	3. REPORT TYPE AND DATES COVERED
	15 Feb. 1998	Annual 15 Oct. 94 - 15 Feb. 98

4. TITLE AND SUBTITLE
Enhanced Correlated-Charge Field Emission

5. FUNDING NUMBERS
C: F49620-95-C-0005

6. AUTHOR(S)
Melvin A. Piestrup,[1] Harold E. Puthoff,[2] Paul J. Ebert[3]

7. PERFORMING ORGANIZATION NAME(S) AND ADDRESS(ES)
[1]Adelphi Technology, Inc.
2181 Park Blvd.
Palo Alto, CA 94306

NE

8. PERFORMING ORGANIZATION REPORT NUMBER

9. SPONSORING / MONITORING AGENCY NAME(S) AND ADDRESS(ES)
Air Force Office of Scientific Research
110 Duncan Ave. Room B115
Bolling AFB DC 20332-8080

10. SPONSORING / MONITORING AGENCY REPORT NUMBER

11. SUPPLEMENTARY NOTES (Consultants)
Authors 2 and 3 from: [2]Institute for Advanced Research
4030 Braker Lane West, Suite 300
Austin TX 78759

[3]Nolasco Science Consultants
1748 Applewood Rd.
Baton Rouge LA 70808

12a. DISTRIBUTION / AVAILABILITY STATEMENT
Unlimited

12b. DISTRIBUTION CODE

13. ABSTRACT (Maximum 200 words)
We have studied the harmonic content of current generated by a field emitter in order to determine if there is spatial or temporal coherence between the electrons. Harmonic content was observed to be identical and high (2nd harmonic/fundamental < 0.45) for both high rates (16,000 events/sec) and low rates (15 events/sec). Statistical analysis shows harmonic content cannot be attributed to the counting system response, but must be considered as true events in which multiple electrons arrive at the detector. Using a single emitter, we compared the spatial distribution of the thermal emission (TE) with that of the field emission(FE). The two profiles were identical; hence, the TE and FE sources were at the same location. Thus multiple electron emission spectra were not a result of parasitic secondary electron emission from intermediate electrodes or other surfaces. We examined the harmonic content by expanding the beam relative to the detector size. The harmonic content was larger than what one would expect if the spatial distribution of the electrons was entirely random, but not big enough to show spatial coherence. We analyzed charge confinement by van der Waals forces which showed that only large numbers of charges can be spatially correlated. Contamination of the FE surface by absorption is suggested as the origin of the multiple-electron emission.

14. SUBJECT TERMS	15. NUMBER OF PAGES
Field emission, electron, charge cluster, plasma, harmonics van der Waals force, Casimir, Spindt Cathode	20
	16. PRICE CODE

17. SECURITY CLASSIFICATION OF REPORT	18. SECURITY CLASSIFICATION OF THIS PAGE	19. SECURITY CLASSIFICATION OF ABSTRACT	20. LIMITATION OF ABSTRACT
Unclassified	Unclassified	Unclassified	SAR

Table of Contents

1. Introduction

Electron field emission has been studied under a variety of experimental conditions. For the purposes of this discussion, we consider three levels of electron beam current: (a) low current where isolated emission events can be counted[1-19]; (b) moderate current where sporadic, noisy pulses are recorded with current measuring devices[20, 21]; (c) high current where plasma effects generally dominate[22-30] and plasma diagnostic techniques are employed. It has not been generally recognized that seemingly unrelated observations of electron clustering in the three current regimes may be governed by similar or related physics.

At low current, researchers were able to measure electron energy and hence spatial and temporal correlation between charges in isolated particle counting events. Herrmann and, later, Gazier first studied individual events using energy-dispersive detectors[1,2]. Gazier detected field-emitted multiple-electron events (2 to 5 electrons) originating in a region of less than 1 mm. Fursey has carried out extensive research in this area over the past two decades[3-14]. He and his colleagues have evaluated the effects of the field emitter temperature, emitter material composition and orientation, and pressure. They also investigated the influence of adsorption of residual gases on the harmonic content of the field emission, since this seemed important in the explanation of Gazier's experiments. Fursey's early results indicated field emission was of single electron character only (no harmonics). This lead to the conclusion that Gazier's results were artifacts connected with parasitic secondary emission from the intermediate electrodes[14]. James and co-workers undertook similar experiments with a thin-window proportional counter[15-18]. Their results also supported Gazier's experiment, as do the results reported herein and in [19]. A summary of low-current experimental results is tabulated in Table I. [19]

In the moderate current regime, emission current from field emitters (Spindt cathodes) is sporadic[20]. Single molybdenum tips exhibit burst (popcorn or telegraph) noise that consists of sequences of bi-stable current pulses of specific amplitude, but with random lengths and random intervals between pulses. These current pulses are separated by quiescent periods, which may be of the order of tens to hundreds of seconds. Current measurements of single Spindt cathodes are in the 10^{-6} to 10^{-8} A range. The burst noise sequences themselves may last from milliseconds to hours. As the resolving time is made shorter, burst current pulses are seen to consist of pulses of similar character, with a limiting pulse length on the order of milliseconds according to Kirton and Urens [21].

In the high current regime, experiments by Shoulders have indicated that high-density spherical charge clusters are possible [22-24]. His work in this area was limited to techniques that are more heuristic than would be desirable for proof of their existence. Shoulders' evidence that field emitted electrons were clustered is both passive (the form of craters on anode surfaces) and active (photographs with a high speed camera). Experiments and modeling which used more conventional plasma physics to describe the presence of spherical impact craters were reported by Schwirzke et al. [29]. They observed circular cratering of both anode and cathode, and their explanation for this emission is quite different from Shoulders' [22]. Theoretical discussions of electron clustering were published by Beckmann, Aspden [25,26] and by Ziolkowski and Tippett[27,28]. Given the nature of Coulomb repulsion, it is difficult at first glance to understand spatial clustering of high current electrons without charge neutralization by trapped ions or image charges. However, as shown by these researchers[25-28] and us[32] other mechanisms for clustering are possible. See sect. 4.

A survey of the literature suggests that researchers in these three different current regimes were not generally aware of each other's work. To clarify some of these issues, experiments in the low current regime were undertaken with an energy dispersive Si surface barrier detector to determine both the temporal and spatial characteristics of thermal and field emission from single, isolated W tips.[19,30]

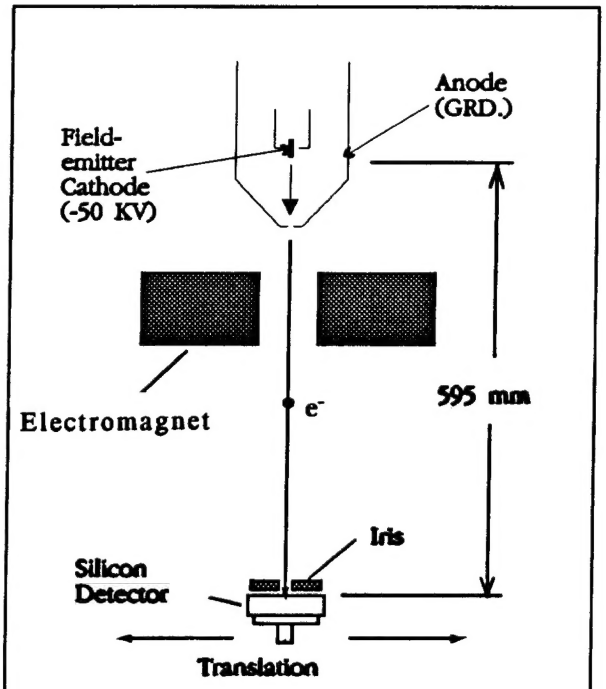

Fig. 1. The Apparatus to study charge correlation.

2. Experiments

2.1. Apparatus

We utilized a modified transmission electron microscope to observe the energy spectra from a point tungsten filament. The experimental apparatus is shown schematically in Fig. 1. The electron source was standard, a commercially available W point filament that could be heated to 2800°K. Thus, the filament could be either a thermal emission (TE) or field emission (FE) source. The tip was positioned in the high field acceleration region of the microscope, through the cathode's aperture. There were no intermediate electrodes between the tip and the anode, which was held at ground potential. All beam optical components such as apertures and magnetic lenses were downstream of the anode. To center the beam on the axis of the microscope, the tip could be shifted in relation to the anode in two normal directions without breaking vacuum. The microscope was operated at 50 kV, and was evacuated with an oil-diffusion pump. Operating pressure was 5 x 10^{-5} Torr or below. The microscope

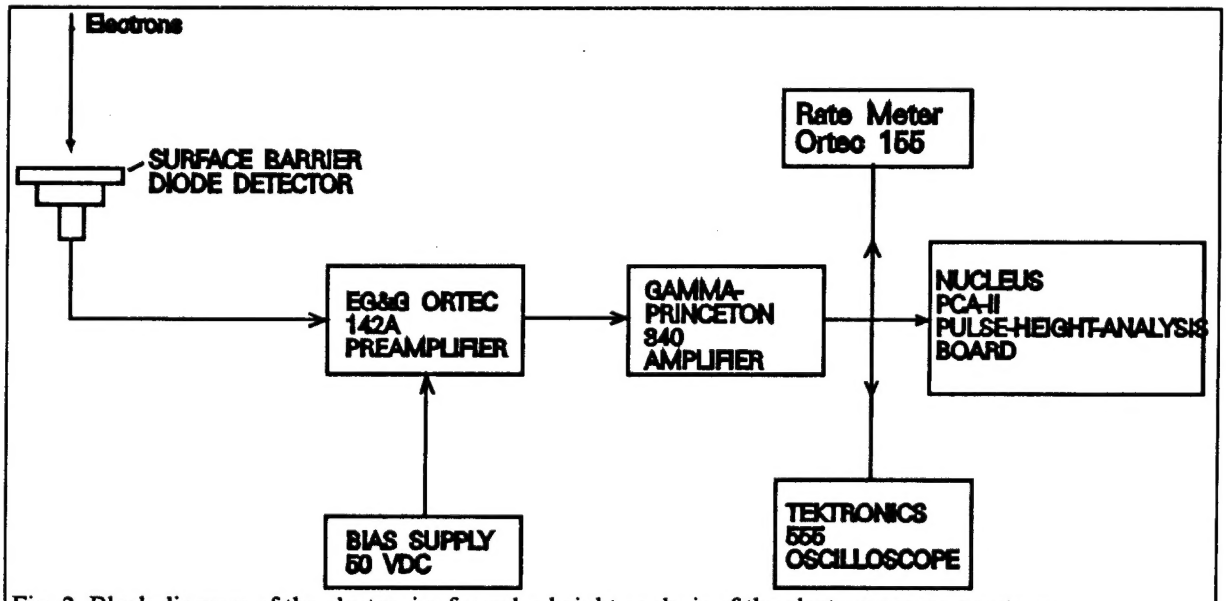

Fig. 2. Block diagram of the electronics for pulse height analysis of the electron energy spectrum.

column had to be extended to accommodate a 25 mm^2 Si surface barrier detector that could be

translated 100 mm along a horizontal axis. The detector was 595 mm from the tip, and was collimated with a 3-mm diameter iris to reduce the active detection area and to improve spatial resolution. The dimensions of the electron beam were controlled with the magnetic lens, and could be viewed with a retractable phosphorescent screen located 25 cm upstream of the detector. Charge pulses from the detector were processed in a counting system (see Fig. 2) consisting of a preamplifier, a main amplifier, a multichannel analyzer and a count rate meter. Amplified pulses (~ 3×10^{-6} sec) were also monitored with an oscilloscope.

Table I. Compilation of experimental results.

Experimenters	T_e-kV	Z	N	n	P-Torr/T-°K	Detector comments
Herrmann[1]	15	W	1	1	10^{-6}/300	proportional ctr.
Gazier[2]	40	W(Th)	5	1.3	10^{-6}/300	cooled Si(Li)
"	"	W	5	1.5	"	"
"	"	Pt	6	1.5	"	"
"	"	Cu	3	1.24	"	cooled Si(Li) low count rate
Fursei[3]	12	Si	4	1.41	10^{-9}/300	Si-surface barrier
Fursei[4]	"	W	2	1.03	"	"
Fursei[5]	17	W	1	1	10^{-10} 77 - 1000°K	Si-surface barrier; many facets of clean W single crystal
Fursei[10,11]	10	W	1	1	10^{-9}	Si-surface barrier; high current, $\Delta t = 10^{-10}$ sec.
Fursei[9]	20	ceramic	4	1.1	10^{-9} 4.2°K	Si-surface barrier, $YBa_2Cu_3O_{7-\delta}$ B = 1 T
Ebert[15]	30	W	6	1.7	10^{-4}/300	Proportional Ctr.
"	40	"	6	1.4	"	"
"	"	"	6	1.5	10^{-6}/300	cooled Si(Li)
James[16-18]	9 to 30	W	6	1.4	10^{-6}/300	75-μm-diam. Prop. Ctr.
This work	50	W	11	1.6	10^{-5}/300	Si-surface barrier

N = number of multiple electron peaks in the measured spectrum.
n = average number of electrons detected per count in the measured spectrum.

2.2 Counting system behavior

Because the spectra reported herein have unusual characteristics (up to 11 electrons arriving simultaneously), it is important to briefly consider the characteristics of our counting system[32]. A count is a pulse that is registered in response to the deposition of energy in the detector. The detector is energy dispersive and linear, that is, the amplitude of the charge pulse generated in it is directly proportional to the energy deposited by the electron(s). Also, there is a fixed minimum time interval that separates two events such that they are recorded as separate pulses. During this interval, the system is "dead." Two electrons arriving during the "dead" time are recorded as a

sum pulse, a single pulse with twice the energy. We were concerned that the counting system might have been overwhelmed by the high rates at which data were accumulated, thereby giving rise to an inordinately large number of sum pulses.

Let the system resolving time be t, and the count rate for random emission of single electrons be r, then the probability of detecting n electrons within t is given by[32]

$$P_n(t) = (2rt)^n / n!$$

and $R_e(n)$, the expected ratio of counts of n electrons to single electron counts is

$$R_e(n) = (2rt)^{n-1} / n!.$$

Values of $R_e(n)$ are given in Table 2 for count rates of 15 and 16,500 counts/sec, and system resolving time of 3×10^{-6} sec.

3. Experimental Results

3.1. Pulse height spectra

Electron-energy spectra were accumulated under several experimental conditions. The count rates were erratic and not controllable over the long term; however, count rate was monitored for stability during data collection. Fig. 3 shows spectra acquired at two vastly different count rates with the cathode at room temperature. The spectrum in 3(a) was taken over a 15 minute period at a count rate of 16,560 counts/sec, while spectrum 3(b) was taken over a 4.75 hour period at a count rate of 15 counts/sec. The lowest energy peak is at 50 keV, and higher energy peaks are at integral multiples of the acceleration voltage. Peaks are observable out to 550 keV, but the acceleration voltage was only 50 keV. The two spectra are similar, and are very much like those obtained by Gazier,[2] Ebert[15] and James, et al.[16-18] Note that in the high count rate spectrum, the gain is shifted to slightly lower energy and peak energy resolution is poorer, suggesting that the counting system was well behaved and was operating properly. Also note that if the multiple energy peaks resulted from counting random single electron emission events in coincidence, then R(n), the ratio of counts of n elections to counts of a single electron would also be given by equation (2). Measured values $R_m(n)$ are compared with expected values $R_e(n)$ in Table 2. These were obtained by adding counts in each peak and subtracting the monotonically decreasing background. The measured values are orders

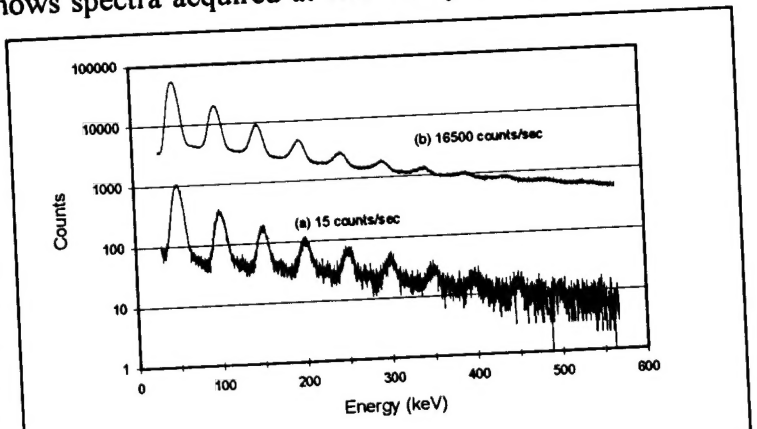

Fig. 3. Pulse height spectra taken from the same field emitter but at different rates: 16,500 counts/sec and 15 counts/sec.

Table 2. Expected and Measured Peak Ratios

Peak No.	Energy	15 Counts/sec.		16500 Counts/sec.	
n	(keV)	$R_e(n)$	$R_m(n)$	$R_e(n)$	$R_m(n)$
1	50	1	1	1	1
2	100	5.0×10^{-5}	3.0×10^{-1}	5.0×10^{-2}	3.5×10^{-1}
3	150	1.4×10^{-9}	1.4×10^{-1}	1.6×10^{-3}	1.2×10^{-1}
4	200	3.0×10^{-14}	7.2×10^{-2}	4.0×10^{-5}	5.3×10^{-2}
5	250	5.5×10^{-19}	4.0×10^{-2}	8.0×10^{-7}	2.0×10^{-2}
6	300	8.2×10^{-24}	2.2×10^{-2}	1.3×10^{-8}	8.1×10^{-3}

of magnitude greater than those expected. The value $R_m(2)$ at 16500 counts/sec is higher than the corresponding value for 15 counts/sec. This is consistent with a higher number of random coincidences at the higher count rate. The differences for the other harmonics are smaller and are within the experimental errors for these ratios. Also, the average number of electrons detected per event was 1.7 ± 0.1 at 15 counts/sec and 1.6 ± 0.1 at 16500 counts/sec. Therefore the multiple energy peaks must be from simultaneous emission of more than a single electron.

3.2. FE and TE source comparison

The microscope's magnetic objective lens was used to demonstrate that the source of multiple electron emission (the FE source) was the tungsten tip. First, with the filament heated, the TE electron source was imaged on the phosphorescent screen, and its position and size checked. The detector was then translated through the beam and the beam profile measured. Next, the filament current was turned off, the count rate meter's discriminator was raised to count pulses that were double energy and higher, and the beam profile of double energy and higher pulses was measured. The two profiles were virtually identical[19]. To obtain higher spatial resolution, the iris sizes were reduced. The diameter of the iris for measuring TE was ~ 100 μm, while that for FE was 2 mm. The electromagnet was turned off to let the electron beam expand. With the filament off, the beam profile of double energy counts was measured (using counts from the pulse height analysis spectrum) and compared with that of the TE profile (using the count rate meter). As is evident in Fig. 4, the normalized profiles for the TE and FE distributions are nearly the same. The difference in resolution of the FE and TE distributions was due to the differing iris sizes. Thus the TE and FE sources were at the same location.

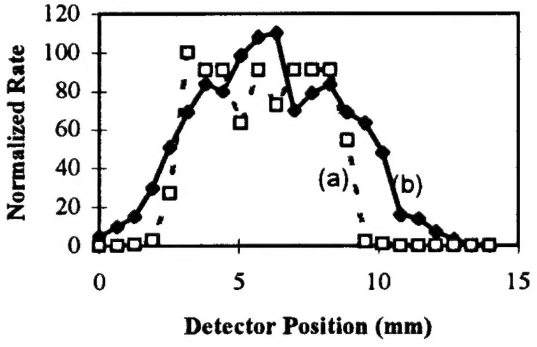

Fig. 4. The normalized count rate of electrons for the cases of (a) thermal emission and (b) the field emission from harmonics above the fundamental both originating from a W point filament. A 2-mm iris was used to measure the FE rate (≥ 2nd harmonic) and a 100 μm iris was used to measure the TE rate.

3.3. Effect of temperature on FE

The emission rate also depended on the temperature of the field emitter. In this experiment, we utilized the fact that the tungsten field emitter could also be operated as a thermal emitter of electrons. We found that the rate of emission increases with increased temperature; however, the ratio of harmonics to the fundamental decreases as the emitter temperature increases. The FE rate could

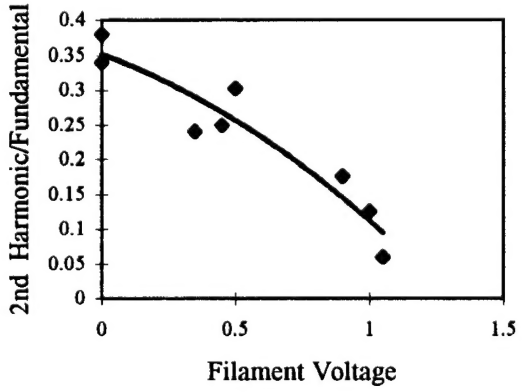

Fig. 5. Harmonic content as a function of filament voltage.

be overwhelmed by increasing the filament current, as can be seen in Fig. 5, which plots the ratio $R_m(2)$ as a function of filament voltage. The beam is nearly 100% thermal at 1.1 volts across the filament. The rate of emission over the 1.1 volt range varied from a few events/sec up to 10^5 events/sec (the limit of the detector electronic's resolution). Thus although the relative harmonic content decreased, the overall rate of harmonic generation increased with increasing temperature.

3.4. Effects of detector aperture size

In our first experiment to explore the possibility that the electrons are spatially correlated, we increased the area of the electron beam so that it was much larger than the area of the Si detector aperture. The assumption was made that loss of higher harmonics would occur if the electrons were not spatially bound. If this was indeed the case, the electrons would have independent trajectories and would result in fewer counts in the harmonics relative to the fundamental. If the electrons are strongly correlated spatially, they will stay together with the same trajectory. Thus the energy spectrum of the increased area beam should still have a high harmonic content.

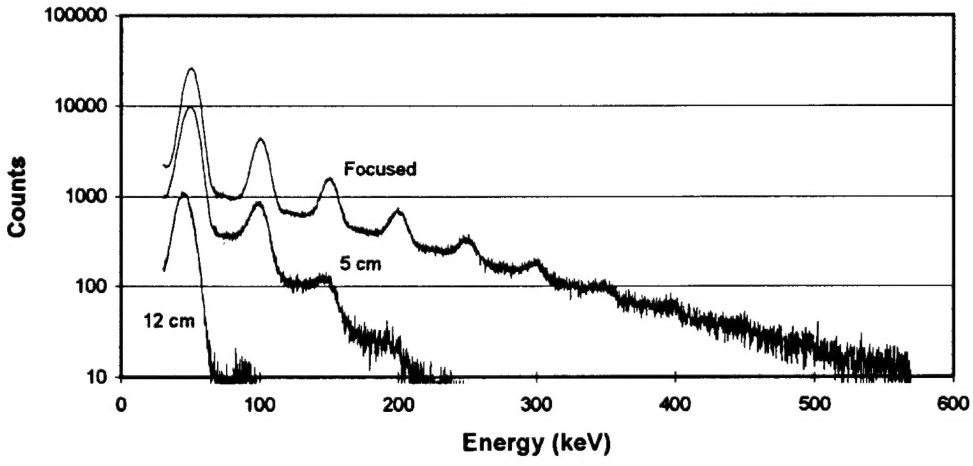

Fig. 6. Pulse height spectrum from a tungsten field emitter for the cases of focused, 5 cm and 12 cm spot sizes at the detector. Detector active area is 25 mm^2.

By simple calculation we can estimate the harmonic content of the beam. Assuming that the electrons stay completely correlated, the expanded electron beam would have the same harmonic content as in the case where the entire beam is focused on the detector. Measurements for the focused case showed that the ratio of the 2nd harmonic to the fundamental was 0.38. Thus, if the electrons remained totally spatially coherent, expanding the area of the beam at the detector would only reduce the rate of detection, not the harmonic content, and the ratio should remain 0.38. On the other hand, if the electrons were moving totally independently of one another, then the harmonic content would be reduced by the ratio of the area of the detector to that of the expanded area.

The pulse height spectra for the cases where the beam is focused onto the detector and where the beam's spot size is increased to 5 cm and 12 cm diameter are shown in Fig. 6. Both the rate and the harmonic content are seen to drop with increasing beam area. The measured ratio of the 2nd-harmonic/fundamental was 0.38 for the case where the electron beam was focused into the detector. Since the active area of the detector was 25 mm^2 (5.6 mm diameter), while the expanded electron beam at the detector was 1962 mm^2 (5 cm diameter), we should expect the 2nd

harmonic/fundamental to be (25/1962) x 0.38 = 0.005 for the case of spatially uncorrelated electrons. For the 5 cm beam, the measured ratio of the 2nd harmonic to the fundamental was 0.08, a factor of 4.7 less than that of the focused case, but a factor of 16 higher than the incoherent case. Thus, the electrons show partial spatial coherence even after traveling a distance of 59.5 cm from the field emitter to the detector. The measured ratios of the 2nd harmonic/fundamental for the 5 cm and a 12 cm diameter spots are given in Table 3.

Table 3: Harmonic Content, Measured vs. Expected

Beam Size (mm) at the detector	2nd har./fund. measured	2nd har./fund. Expected value if no spatial coherence
focused	0.38	0.38
5 cm	0.08	0.005
12 cm	0.008	0.0008

3.5. Electron beam size reduction

To see if the magnetic focusing contributed to the increased randomization of the electron beam, we utilized the apertures (1.3 mm and 0.65 mm diameter irises) of the cylindrical magnet (with magnet off) to define the size of the electron beam. The electron beam was allowed to naturally expand as it traveled to the detector. The measured size of the electron beam at the detector was 1 cm. The irises could be placed 27.8 cm from the field emitters and 48.4 cm from the detector. In this experiment the detector was 762 mm from the source. We estimate the spot size of the beam to be 5 mm at the iris. As discussed above, limiting the size of the electron beam should not reduce the harmonic content if the electrons are highly spatially correlated. The results are shown in Fig. 7, where we compare three spectra, one with no aperture, one with 1.3 mm and one with 0.65 mm. The expected and the measured 2nd harmonic/fundamental ratios are given in Table 4. The expected value for no spatial coherence are calculated by assuming that the harmonic content is reduced by the ratio area of the irises to that of the area of the electron beam. Again the measured values show a degree of spatial correlation. For both irises, the measured ratio was a factor of 10 or more higher than the expected value if the electrons were uncorrelated.

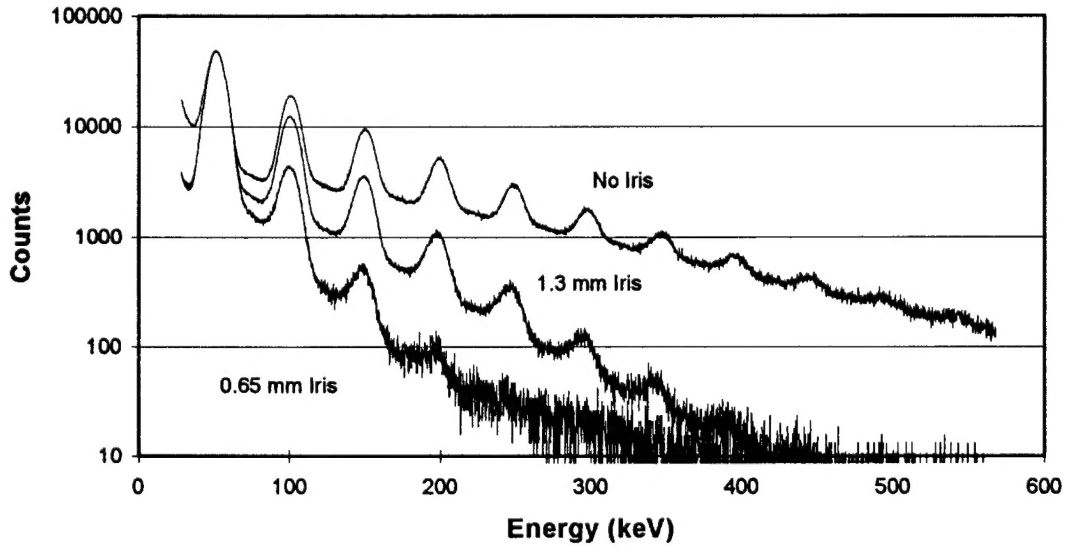

Fig. 7. Pulse height spectrum from a tungsten field emitter for the cases of no iris and 1.3 mm, and 0.65 mm irises.

3.7. Temporal behavior of harmonic FE.

A Nuclear Instruments multi-channel scalar (MCS) was utilized to determine the change in harmonic content as a function of time. We looked at both short term ($t < 300$sec) and long term response ($\Delta t \approx 1$ hour) of the FE. A number of experiments were done using the several different field emitters at several different temperatures and vacuums. Results show that the age of the field emitter, its vacuum, and its possible poisoning by gas absorption determine the field-emission rates.

Table 4: Harmonic Content, Measured vs. Expected

Iris Size (mm)	2nd har./fund. measured	2nd har./fund. Expected value if no spatial coherence
focused	0.38	0.38
1.3 mm	0.26	0.025
0.65 mm	0.09	0.006

3.8. Long term time response of harmonic content

We utilized a new field emitter (bent W wire) commonly used in electron microscopes. The field emission was first observed using our standard pulse height analysis (PHA) setup (Fig. 2) and a PHA electron-energy spectrum was taken to make sure there was harmonic content to the emission. The usual PHA spectrum (like Fig. 3) was seen. The pulse-height-analysis (PHA) board was then set in the multi-channel scalar (MCS) mode with the dwell time set for 1 sec. In the MCS mode, the count rate could be measured and recorded as a function of time. The discriminator of the PHA board was then set above the fundamental; thus the MCS was only counting events with multiple electrons in each event. The MCS was done immediately after the PHA spectrum. Thus the field emitter had been used for over an hour. As can be seen from Fig. 8, there was a long term decay from 600 counts/sec to 400 counts/sec. Approximately three hours later, the MCS was again taken and the rate had become an average constant rate of 127 counts/sec.

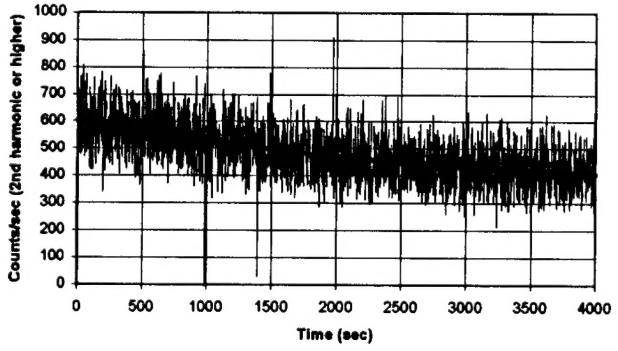

Fig. 8. The number of counts/sec of multiple-electron emission in single field-emission events as a function of time. This data was taken in the first hour of the field emitter life.

3.9. Short Term Time Response of Harmonic Content

The field emission rate was observed after what we determined was the deliberate poisoning of the field emitter by heating the filament to thermal emission temperatures in a poor vacuum (6×10^{-6} Torr). The filament temperature was then reduced and the count rate measured as a function of time. The field emission harmonic content rate was found to be high but decaying rapidly. For the particular example shown in Fig. 9, the rate drops from approximately 1000 counts/sec to 100 counts/sec in approximately 180 sec, finally reaching a low, constant rate of 20 counts/sec after about 300 sec. The field emitter used here had been used for many hours and had

a lower constant rate than the one used in Figs. 2-4 and did not exhibit the long term behavior of these Figs.

A heated field emitter (one whose termperature is below thermal emission temperatures) also showed similar harmonic rate changes for both long and short terms. Note that a completely thermalized field emitter does not show this behavior. An example of this measurement is shown in Fig. 10. The same field emitter used in Fig. 9 was used. The cathode was first heated to thermal emission temperatures (1.6 VDC). The filament voltage was then reduced to 0.8 VDC and the count rate measured as a function of time. Rate is seen to dramatically drop from 7000 counts/sec to 700 counts/sec in approximately 170 sec.

Two interesting effects are observed when comparing Fig. 9 and 10. First, the harmonic rate is higher (but not the harmonic content), and, secondly, the average deviation of the rate is smaller for thermalized FE. The latter becomes more apparent when we compare these Figs. For any possible applications of multiple electron FE, control over the harmonic content of FE is important.

Higher quality vacuum saw also used to determine how the multiple emission was affected. A turbo pump was utilized to improve our vacuum to 10^{-7} Torr. Early measurements showed the multiple emission to disappear; thus, our measurement agreed with Fursei's results, which saw multiple-electron emission disappear with higher quality vacuums (10^{-10} Torr).

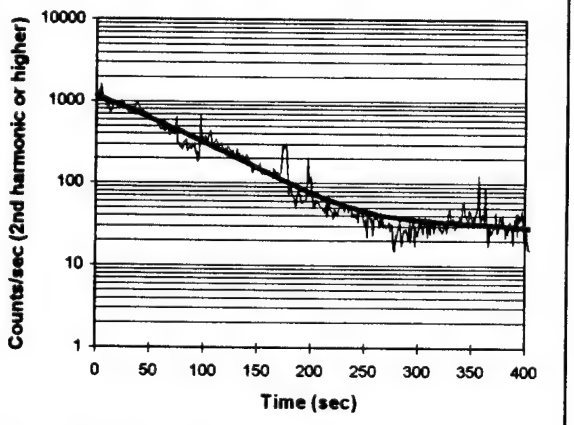

Fig. 9. Short term time response of a field emitter. Room temperature field emitter.

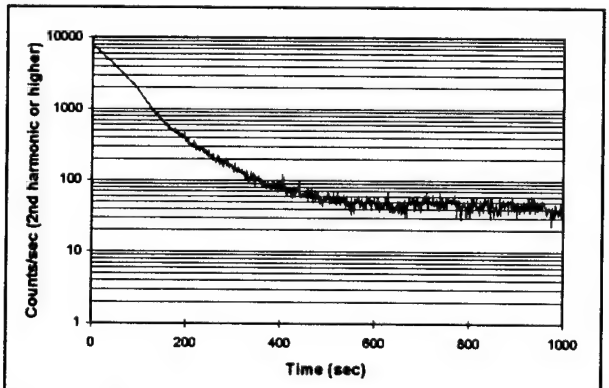

Fig. 10. Short term time response of a field emitter that has been heated (cathode voltage is 0.8 VDC) but emission is not thermal.

3.10. Attempts of to observe spatial coherence

Based on our early calculations showing possible charge clustering, we attempted to observe spatial coherence effects. The assumption was that if the electrons were tightly spatially clustered after emission, then they would behave as a large single particle whose charge was ℓ e and mass was ℓ m, where is the number of electron in the cluster.

The experiment was designed to reduce the upper limit on the size of the correlated charge cluster to less than 2 Å. The experiment utilized Bragg scattering of electrons from silicon. The ELMISKOP II has the ability to Bragg scatter the electrons off of crystal. We have already observed electron diffraction off of silicon <111> and <001>. The Bragg angle is proportional to the de Broglie wavelength of the charged particle that is to be scattered. Assuming the mass and charge are proportional to ℓ, the Bragg angle goes as:

$$\theta_B = \frac{12.3n}{2d(\ell E)^{1/2}}$$

For silicon <111> with the 220 reflection (d = 1.92Å), n = 1, and E = 50 keV, the Bragg angles for $\ell = 1,2,3$ are θ_B = 14.3, 10.1 and 8.2 mrad, respectively. Thus, the Bragg-scattered electrons will scatter at different angles depending upon the cluster size ($\ell = 1,2,3,...$).

Our attempts to observe this effect both visually and with our translatable Si detectors met with negative results. However, the electrons will be scattered at different angles from the fundamental ($\ell = 1$) only if the distance between them is much less than the lattice spacing of the crystal (in this case 1.92 Å). Thus this negative results can be said to show that the electron were not spatially correlated below few angstroms.

4. Possible Mechanism for Charge Confinement

4.1. Introduction

Laboratory observation of high-density filamentation or clustering of free electronic charge by Shoulders and others indicates that under certain conditions strong coulomb repulsion can be overcome by cohesive forces as yet imprecisely defined. [22-29] Such spatial clustering may occur at any of the suggested electron densities as discussed in the Introduction (sect. 1). Aside from the case of electron charge neutralization by positive ions, mechanisms proposed in the literature for high-density charge confinement range from standard magnetic pinch models to exotic, soliton-like localized-wave (LW) solutions in plasma-EM wave interactions[27-28].

Another candidate mechanism that has yet to be fully explored with regard to charge confinement is provided by the short-range, attractive van der Waals and Casimir forces driven by vacuum-fluctuation phenomena. Such forces derive from the fact that the vacuum, rather than being the void of classical theory, is the seat of electromagnetic zero-point fluctuations (ZPF) of enormous energy density and radiation pressure. Theory predicts and experiments verify the existence of the van der Waals-type forces between closely-spaced metallic or dielectric boundaries, and between free charge distributions. One example is the Casimir force, the attractive, ZPF-induced quantum force between conducting parallel plates[34-37], recently measured with good precision[38]. Detailed analysis shows that the attractive force is due to a partial shielding of the ZPF radiation pressure from the interior region of the plates, which results in the plates being pushed together[39].

As to the issue of charge confinement specifically, it was Casimir himself who first proposed that the ZPF-induced pressure forces might provide a mechanism for the confinement of charge in (semi-classical models of) elementary particles, a problem even more challenging than the laboratory one under consideration here.[40] To explore this concept in some detail here we examine, first, the lower limiting case of the van der Waals attraction between two isolated charges, and then the collective behavior involving multiple charge distributions of various geometries.

4.2. Two-particle van der Waals force interaction

The ZPF-induced van der Waals interaction between a pair of polarizable particles is given by [41-43]:

$$U_{vdw}(R) = \mathrm{Re}\left\{-\frac{\alpha^2\hbar c}{\pi}\int_0^\infty du \frac{u^4\omega_0^4}{(c^2u^2+\omega_0^2)^2}\frac{e^{-2uR}}{R^2}\left[1+\frac{2}{(uR)}+\frac{5}{(uR)^2}+\frac{6}{(uR)^3}+\frac{3}{(uR)^4}\right]\right\} \quad (1)$$

where $\alpha = q^2/4\pi\varepsilon_O m\omega_O^2$ is the static polarizability of each particle, and $u = -ik = -i\omega/c$.

For a free particle (electron) $\omega_0 \to 0$, and the above can be simplified to

$$U_{vdw}(R) = -\frac{9}{4}\frac{\hbar c^3\Gamma^2}{\pi R^3}\int_0^\infty dx\left[\sin(2x)+\frac{2\cos(2x)}{x}-\frac{5\sin(2x)}{x^2}-\frac{6\cos(2x)}{x^3}+\frac{3\sin(2x)}{x^4}\right], \quad (2)$$

where x = kR and $\Gamma = q^2/6\pi\varepsilon_o mc^3$.

Term by term integration then leads to an expression of the form (with y = 2x)

$$U_{vdw}(R) = -\frac{9}{4}\frac{\hbar c^3\Gamma^2}{\pi R^3}\left[\frac{1}{2}\int_0^\infty dy \sin y+\frac{2}{3}\right]. \quad (3)$$

The final step in the evaluation of the integral is to realize that at some high frequency the free-electron response to the ZPF can be expected to drop off. Thus we can insert an integrating factor of the form $e^{-\lambda y}$ into the integrand in (3) and then let $\lambda \to 0$ after the calculation,

$$\lim_{\lambda\to 0}\int_0^\infty dy e^{-\lambda y}\sin y = \lim_{\lambda\to 0} Im\int_0^\infty dy e^{(-\lambda+i)y} = \lim_{\lambda\to 0}\left[-Im\frac{1}{-\lambda+i}\right]=1, \quad (4)$$

yielding for the final result

$$U_{vd\omega}(R) = -\frac{21}{8}\frac{\hbar c^3\Gamma^2}{\pi R^3}. \quad (5)$$

An excellent overview placing such calculations within a broad context of particle interactions is provided by Spruch[44].

We are now in a position to inquire as to the close-approach distance where, aside from other considerations, the repulsive coulomb force would be overcome by an attractive van der Waals force as calculated here. The total potential for the two can be written in the form

$$\frac{U(R)}{m_e c^2} = \frac{r_e}{R}-\frac{7}{6\pi}\left(\frac{\hbar/m_e c}{r_e}\right)\left(\frac{r_e}{R}\right)^3, \quad (6)$$

where $(\hbar/m_e c)$ and r_e are, respectively, the Compton and classical electron radii. The total force F, given by $F = -dU(R)/dR$, would go to zero (forces would balance) at $R \sim 12.4\, r_e \sim 3.5 \times 10^{-14}$ m. Having completed this calculation, however, we recognize that we have exceeded the limits of applicability of such a simple model of van der Waals capture and confinement; e.g., confinement at such close spacing would be opposed by yet another "force," the so-called "Schrödinger pressure." The Schrödinger pressure, about which more will be said in the following section, is a force that resists particle confinement due to the wave nature of matter that can be seen as deriving from a combination of the uncertainty and Pauli exclusion principles[45]. Balance of this force $\left(\approx \hbar^2/mR^3\right)$ by the van der Waals force cannot be achieved under realistic conditions, and so we must turn to the multiparticle case for such a possibility.

4.3. Multiparticle van der Waals/Casimir-force interaction

Early investigation by Casimir of vacuum-fluctuation-driven, multiparticle van der Waals interactions led to the realization that summation over the collective particle-particle interactions could be recast to advantage in terms of the restructuring of vacuum energy in response to the boundaries defined by the particle distributions[34]. This is because charge distributions which can respond to fields constitute boundaries which reconfigure those fields, vacuum ZPF fields included. The classic example is the Casimir effect mentioned in the Introduction. Conducting parallel plates exclude all but a finite number of modes in the interior spacing, with the consequence that the radiation pressure outward on the plates associated with the interior modes is less than the pressure inward due to the (essentially infinite in number) external modes. This yields a net radiation pressure which drives the plates together with a force per unit area given by[39]

$$\frac{F}{A} = -\frac{\pi^2}{240}\frac{\hbar c}{d^4}, \tag{7}$$

where d is the spacing between the plates.

With regard to the containment of high-density charge, originally of interest for the development of semiclassical models of elementary particles, Casimir suggested that a shell-like distribution of charge might partially shield vacuum fields from the interior of the shell with the result that net inward radiation pressure would compensate outwardly-directed coulomb forces to yield a stable configuration at small dimensions. Along these lines Casimir offered two models for consideration[40], one which assumes total shielding of interior fields up to a Compton-frequency cutoff for electron-ZPF field interactions, and a second in which interior fields associated with discrete states permitted by boundary conditions are assumed to exist, as in the parallel-plates example above. We examine both possibilities here.

4.4. Casimir's shell model I

The plausibility of Casimir's first model (total shielding of interior fields up to some cutoff frequency) finds some support in recent work by one of the authors (H.P.). This work traces the source of ZPF fields to the quantum-fluctuation motion of charged particles distributed over cosmological space[46]; such fields could then in principle be shielded from an interior space by a sufficiently dense charge distribution.

With the spectral energy density of the ZPF fields given by

$$\rho(\omega)d\omega = \frac{\hbar\omega^3}{2\pi^2 c^3}d\omega, \tag{8}$$

integration over frequency from zero up to a cutoff frequency Ω_c for electron-ZPF interactions yields a vacuum energy density u_V effective in such interactions,

$$u_v = \int_0^{\Omega_c}\rho(\omega)d\omega = \frac{\hbar\Omega_c^4}{8\pi^2 c^3}. \tag{9}$$

Now assume a spherical-shell distribution of N electrons on a shell of radius a. For the ZPF radiation pressure to compensate the electrons' coulomb stress, we require (1/3) $u_V = u_e$, or

$$\frac{1}{3}\frac{\hbar\Omega_c^4}{8\pi^2c^3}=\frac{1}{2}\varepsilon_0E^2=\frac{N^2\alpha\hbar c}{8\pi a^4}, \tag{10}$$

where here α is the fine structure constant, $\alpha=e^2/4\pi\varepsilon_0\hbar c\approx 1/137.036$. This leads to an expression for the cutoff frequency,

$$\Omega_c=(3\pi\alpha)^{1/4}\sqrt{N}\left(\frac{c}{a}\right). \tag{11}$$

Alternatively, the above expression can be derived by equating the ZPF energy missing from the interior of the sphere to that stored in the coulomb field.

With regard to the cutoff frequency Ω_c for electron-ZPF interactions, we choose the Compton frequency defined by $\hbar\Omega_c=m_ec^2$, where m_e is the electron mass. This choice for the cutoff has been shown to yield correct results for other electron-ZPF interactions, for example in calculations of the Lamb shift[47, 48]. Substitution into (11) then yields an expression for the diameter d of the spherical-shell distribution,

$$d=2a=2(3\pi\alpha)^{1/4}\sqrt{N}\left(\frac{\hbar}{m_ec}\right)\approx\sqrt{N}\left(\frac{\hbar}{m_ec}\right). \tag{12}$$

We see that the diameter for the spherical-shell distribution predicted by this calculation is simply the Compton wavelength $\hbar/m_ec$, multiplied by the square root of the number of electrons on the shell. This corresponds to each electron on the shell occupying a circular area with radius approximately equal to the Compton wavelength in an apparent quantum equivalent of close-packing.

As with the two-particle van der Waals interaction, we need to determine whether the Schrödinger pressure plays a significant role in this configuration. The complete expression for the Schrödinger pressure exerted by N free electrons confined to volume V in their lowest energy state (N/2 with spin up, N/2 with spin down) is[45]:

$$P_s=\frac{1}{5}\left(3\pi^2\right)^{2/3}\frac{\hbar^2}{m_e}\left(\frac{N}{V}\right)^{5/3}. \tag{13}$$

A direct comparison of the magnitude of the Schrödinger pressure against the vacuum and coulomb pressures, given by $(1/3)u_V$ and u_e, respectively, indicates that the Schrödinger pressure can be neglected for electron numbers of interest here, say $N \gg 10^4$.

Finally, we note that the spherical-shell configuration envisioned here satisfies the stability condition that a slight change in radius results in a restoring force that tends to return the sphere to its original size.

4.5. Casimir's shell model II

In Casimir's shell model of the second type, in place of the shielding of the interior from all ZPF fields below the Compton frequency, interior fields associated with those discrete states permitted by boundary conditions are assumed to exist, as in the parallel-plates example.

One of the first models of this type to be published in the literature considered a semiclassical electron as a conducting spherical shell carrying a homogeneously-distributed surface charge e, whose tendency to expand by coulomb repulsion is checked by inwardly-

directed ZPF radiation pressure (the Casimir force)[49]. Unfortunately for the model, a detailed analysis found that for this case the Casimir pressure was outwardly-directed, augmenting rather than canceling the coulomb pressure. This type of analysis was then extended to the case of solid dielectric and conducting balls[50]. For these examples the Casimir pressure turned out to be inward as required, but the analysis was still unsatisfactory with regard to certain mathematical divergences and the prediction of an erroneous value for the fine-structure constant.

Of relevance to our interests here, however, is the Casimir-effect solution for a conducting *cylindrical* shell, one of the limited number of geometries for which, fortunately, a solution is available[51]. The reason for this geometry being of interest is the observed tendency for high-density charge distributions to take the form of cylindrical filaments or, in some instances, cylinders wrapped head-to-tail to form toroids. The generation of high-charge-density entities by field emission tips have been reported to favor "smoke-ring" geometries, i.e., toroids[22]. The cylindrical solution yields for the Casimir energy per unit length

$$\frac{E_{cas}}{L} = -\frac{\pi C_1 \hbar c}{a^2} \quad , \tag{14}$$

where a and L are the radius and length of the cylinder; $C_1 = 4.32 \times 10^{-3}$ is a scale factor deriving from detailed analysis of the ZPF field distribution as it matches the boundary conditions imposed by the cylindrical geometry. The associated Casimir pressure (force per unit area), $\left(F_{cas}/A\right) \rightarrow -\left(dE_{cas}/dV\right)$, is in turn given by

$$\frac{F_{cas}}{A} = -\frac{C_1 \hbar c}{a^4} \tag{15}$$

The corresponding expression for the coulomb pressure is:

$$\frac{F_{coul}}{A} = \frac{(Q/L)^2}{8\pi^2 \varepsilon_0 a^2} \tag{16}$$

where (Q/L) is the charge per unit length.

Finally, the Schrödinger pressure given by (13) is found to play a significant role in the filamentary geometry, with its corresponding expression for the cylindrical geometry given by

$$\frac{F_s}{A} = \frac{3^{2/3}}{5\pi^{1/3}} \frac{\hbar^2}{m_e} \frac{1}{a^{10/3}} \left(\frac{N}{L}\right)^{5/3} \quad , \tag{17}$$

where N is the number of charges (electrons) involved, determined by $Q = Ne$.

With the coulomb pressure proportional to $1/a^2$ and the Casimir pressure proportional to $1/a^4$, a diffuse distribution of free charge will simply disperse as the result of coulomb repulsion forces. However, if a cylindrical-shell (straw) filament of electrons reaches a critical threshold density determined by $|F_{cas}/A| \geq |F_{coul}/A|$, or

$$a \leq \frac{\sqrt{2\pi C_1/\alpha}}{(N/L)}, \tag{18}$$

then charge-filament collapse will set in (again, α is the fine structure constant). A quick calculation shows that, for example, 10^4 electrons organized into a 1-μm diameter filament, 2.5-

mm long, would satisfy the condition for filament collapse, while an inch-long filament of this diameter could support 10^5 electrons.

In this model once filament collapse sets in, the $1/a^4$ Casimir pressure overwhelms the $1/a^2$ coulomb pressure, driving the filament diameter to ever-decreasing values and thus higher charge densities. Aside from classical instabilities that are certain to occur, at a formal level a limiting minimum filament diameter is predicted as quantum features emerge, specifically as represented by the Schrödinger pressure. As filament collapse occurs, the coulomb pressure becomes negligible compared to the Casimir pressure, and can therefore be neglected. The Casimir pressure with its $1/a^4$ dependence, if left unchecked, could in principle overwhelm even the Schrödinger pressure with its $1/a^{10/3}$ dependence. However, the $1/a^4$ -dependent Casimir equation, taking into account as it does retardation effects in the electromagnetic field, reverts to a $1/a^3$ van der Waals-type dependence associated with the nonretarded-field solution when separation distances become comparable to the shortest wavelength that can be reflected by the charges constituting the Casimir boundaries[52] (in this case the Compton wavelength of the electrons, as noted earlier); thus the Schrödinger pressure can become effective in preventing further collapse. This transition from a retarded to a nonretarded-solution law can be seen in the experimental data of Israelachvili and Tabor, obtained in experiments involving crossed cylinders of mica as Casimir boundaries[53].

An attempt to go further in applying detailed calculations of the above type to plasma-arc filament formation under complex laboratory conditions is surely not warranted at this point; detailed experimentation specifically to test the van der Waals/Casimir hypothesis will be required. Nonetheless, the theoretical considerations presented here indicate that van der Waals/Casimir-type effects may well play a role in the generation of robust, high-charge-density effects that have been reported in arc-discharge experimentation.

5. Summary of Results

5.1. High harmonic content observed from field emission

We used a Si-surface barrier particle detector to measure electron energy spectra at dramatically differing counting rates.[19] Harmonic content was unusually high, with an average number of electrons per count of 1.6 for high (16,500 events/sec) and 1.7 for low (15 events/sec) count rates. Statistical analysis by us shows that this high harmonic content cannot be attributed to the counting system response, but must be considered as true events in which several electrons are emitted simultaneously and arrive within the resolution time of the detector and its electronics (~3 μsec). As many as 11 electrons were detected in single random-emission events in isolated random field-emission events. Heating the field emitter results in an increase in event rate, but a decrease in the harmonic content of the energy spectrum (reduction in the number of multiple electrons per event).

5.2. Multiple electron emission originates from the field emitter

The event rate of the multiple emission for 2 electrons or more was used to map the spatial distribution of the FE and compared to that of TE. The spatial distributions overlapped closely thus indicating that both emissions were coming from the bent-wire W filament and not from parasitic secondary emission from the intermediate electrodes as supposed by Fursei.[19]

5.3. No attractive force for low numbers of electrons

We investigated possible spatial coherence by measuring the dependence of energy spectra on the area of the electron beam, whose size relative to that of the detector was varied using (1) a cylindrical magnet to increase beam diameter and (2) irises to reduce detector diameter[30], and (3) by attempting to observed Bragg scattering of possible clustered electrons. The harmonic content was larger than what one would expect if the spatial distribution of the electrons was entirely random, but not large enough to indicate that there is any attactive force between the simulateously emitted electrons that would overcome Coulomb repulsion. The Bragg experiments showed that the electron were not spatially correlated below few angstroms.

Since there is no attractive force to keep the electrons together, the use of a cylindrical magnet to collect and focus electrons onto the detector was important to demonstrating temporal correlation. The magnet functions to keep all the simultaneously emitted electrons together so that they will be counted as a multiple electron pulse. Indeed, the experiments of Fursey et al. [3-14] do not appear to use focusing and this may be the reason their results have fewer (and in some cases, no) multiple counts.

A class of models which invoke the possibility of charge confinement by van der Waals-type forces was suggested by Casimir. Our resulting analysis (sect. 4) and the experimental results (sect. 3) indicate that confinement of small numbers of electrons by the van der Waals mechanism cannot be achieved under experimental conditions that we considered. However, large numbers can be clustered by the van der Waals force.[32]

5.4. Emitter impurities appear to improve harmonic content

A distinguishing feature of our experiments that routinely detected multiple emission was that the vacuums were much poorer than in many of Fursei's experiments.[19] Our use of a higher vacuum (10^{-7} Torr) also resulted in reduced event rates of multiple emission. Measurements of the time evolution of the harmonic content shows that there is both long and short term changes in the count rate.[31] Based on these experiments, contamination of the FE surface by absorption of gas molecules is suggested as the origin of the multiple-electron emission.

References

[1] M. Herrmann, "Investigation of different processes of multiple electron emission," Z. Physik **184**, pp. 352-354 (1965). In German.

[2] C. Gazier, "Multiple-electron events from field emission," Phys. Lett. **35A**, pp. 243-244 (1971).

[3] G. N. Fursei, M. M. Mokhasne, N. V. Egorov, V. S. Ponomarev, and V. N. Shchemelev, "Statistics of field-electron emission," Sov. Phys. Solid State **18**, pp. 368-369 (1976).

[4] M. M. Mokhasne, V. S. Ponomarev, N. V. Egorov, G. N. Fursei, and V. N. Shchemelev, "A procedure for investigating the statistics of field emission," Instrum. Exp. Tech. (USA) **19**, pp. 496-498 (1976).

[5] G. N. Fursei, N. V. Egorov and A. V. Kocheryzhenkov, "Field-emission statistics for various faces of a tungsten single crystal," Sov. Tech. Phys. Lett. **7**, pp. 343-345 (1981).

[6] N. P. Afanas'eva, N. V. Egorov, A. V. Kocheryzhenkov and G. N. Fursei, "A method of examining the number of electrons produced in an elementary act of field emission," Instrum. Exp. Tech. (USA) **25**, pp.1204-1206 (1982).

[7] A. V. Kocheryzhenkov, V. I. Maslov and G. N. Fursei, "Statistics of field-electron emission from tungsten and niobium at helium temperatures," Sov. Phys. Solid State **29**, pp. pp. 1421-1422 (1987).
[8] V. I. Maslov, G. N. Fursei, A. V. Kocheryzhenkov, and N. P. Afanas'eva, "Apparatus for study of statistics of field emission at low temperatures," Instrum. Exp. Tech. (USA) **30**, pp. 1162-1164 (1987).
[9] G. N. Fursei, A. V. Kocheryzhenkov, V. I. Maslov and A. P. Smirnov, "Multiparticle tunneling during field emission from $YBa_2Cu_3O_{7-\delta}$," Sov. Tech. Phys. Lett. **14**, pp. 804-805 (1989).
[10] V. I. Maslov, G. N. Fursei and A. V. Kocheryzhrnkov, "Statistics of field emission for tungsten over a wide range of current densities," Sov. Phys. Tech. Phys. **34**, pp. 1192-1194 (1989).
[11] V. I. Maslov, G. N. Fursei and A. V. Kocheryzhenkov, "Investigations of the quantity of elementary acts of field emission with time resolution of 5 μs - 100 ps," J. de Physique **50** C8 supplement, pp. C8-113 to C8-117 (1989).
[12] V. I. Maslov, G. N. Fursei and A. V. Kocheryzhenkov, "Method for study of field emission statistics over a wide current-density range," Instrum. Exp. Tech. (USA) **33**, pp. 395-399 (1990).
[13] G. N. Fursey, A. V. Kocheryzhenkov and V. I. Maslov, "The quantity of elementary acts and the statistics of field emission," Surface Science **246**, pp. 365-372 (1991).
[14] G. N. Fursei, A. V. Kocheryzhenkov, V. I. Maslov, A. L. Shmaev and L. N. Borisov, "Apparatus for study of multiparticle acts of field emission at low temperatures," Instrum. Exp. Tech. (USA) **33**, pp. 152-154 (1990).
[15] P. J. Ebert, (1970). Unpublished experimental results; excerpted from unpublished research proposal (1990).
[16]. F. J. James, LLNL contract report, September 1993. unpublished.
[17] F. James, P. Ebert, T. Miller, K. Wansley and T. Terry, "Production of Multiple Electron Peaks from a Tungsten Electron Gun in Field Emission Mode," Bull. Am. Phys. Soc. **38**, 2174 (Nov. 4-6, 1993).
[18] F. James, "Time Study of Multiple Electron Peaks Produced by a Tungsten Electron Gun in Field Emission Mode," Bull. Am. Phys. Soc. **40**, 952 (1995).
[19]* M. A. Piestrup, H. E. Puthoff and P. J. Ebert, "Measurements of multiple-electron emission in single field-emission events," J. Appl. Phys. Comm. **82**, 5862 (1997).
[20]C. A. Spindt, I. Brodie, L. Humphey, and E. R. Westerberg, "Physical Properties of thin field emission cathodes, with molybdenum cones," J. Appl. Phys. **47**, pp. 5248-5263 (1976).
[21] M. J. Kirton and M. J. Urens, "Noise in solid state microstructures," Adv. in Phys. **38**, pp. 367-468(1989).
[22] K. R. Shoulders, "EV: A Tale of Discovery," (Jupiter Technologies, Austin, TX, 1985).
[23] K. R. Shoulders, "Method of and apparatus for the production and manipulation of high density charge," U. S. Patent 5,054,046.
[24] K. R. Shoulders, "Circuits responsive to and controlled by charged particles," U. S. Patent 5,054,047.
[25] Petr Beckmann, "Electron Clusters," Galilean Electrodynamics, **1** , No. 5, pp. 55-58 (1990).
[26] H. Aspden, "Electron Clusters," Correspondence, Galilean Electrodynamics, **1** , No. 6, pp. 81-82 (1990).

[27] R. W. Ziolkowski and M. K. Tippett, "Collective effect in an electron plasma system catalyzed by a localized electromagnetic wave," Phys. Rev. A, **43**, pp. 3066-3072 (1991).
[28] R. W. Ziolkowski, "Electromagnetic localized waves that counteract Coulomb repulsion to catalyze a collective electron-packet state," Phys. Rev. E, **52**, pp. 5338-5343 (1995).
[29]F. Schwirzke, M. P. Hallal, X. K. Maruyama, "Onset of Breakdown and formation of cathode spots," IEEE Trans. on Plasma Science, **21**, pp. 410-415 (1993).
[30]* M. A. Piestrup, H. E. Puthoff and P. J. Ebert, "Correlated Emission of Electrons" scheduled for publication, Galilean Electrodynamics, May/June 1998.
[31]* M. A. Piestrup and P. J. Ebert, "Temporal behavior of multiple-electron emission in single field-emission events" to be submitted J. Appl. Phys. Communications (1998)
[32]* H. E. Puthoff and M. A. Piestrup, "Charge Confinement by van der Waals/Casimer-Type Forces," Submitted to Phys. Lett. A.
[33] Glenn F. Knoll, **Radiation Detection and Measurement**, 2nd Ed., John Wiley & Sons, New York, 1989.
[34] H. B. G. Casimir, Proc. Kon. Ned. Akad. Wetenschap. **51**, (1948) 793.
[35] M. Fierz, Helv. Phys. Acta **33**, (1960) 855.
[36] T. W. Marshall, Nuovo Cimento **38**, (1965) 206.
[37] T. H. Boyer, Ann. Phys. (N.Y.) **56**, (1970) 474.
[38] S. K. Lamoreaux, Phys. Rev. Lett. **78**, (1997) 5.
[39] P. W. Milonni, R. J. Cook, and M. E. Goggin, Phys. Rev. A **38**, (1988) 1621.
[40] H. B. G. Casimir, Physica **19**, (1953) 846.
[41] T. H. Boyer, Phys. Rev A **7**, (1973) 1832.
[42] M. J. Renne, Physica **53**, (1971) 193.
[43] H. B. G. Casimir and D. Polder, Phys. Rev. **73**, (1948) 360.
[44]L. Spruch, in *Long-Range Casimir Forces: Theory and Recent Experiments on Atomic Systems*, edited by F. S. Levin and D. A. Micha (Plenum, New York, 1993).
[45] V. F. Weisskopf, Science **187**, (1975) 605. See also Am. J. Phys. **53**, (1985) 109, 206, 304.
[46] H. E. Puthoff, Phys. Rev. A **40**, 4857 (1989); Errata and Comments, Phys. Rev. A **44**, (1991) 3382, 3385.
[47] H. A. Bethe, Phys. Rev. **72**, (1947) 339.
[48] T. A. Welton, Phys. Rev. **74**, (1948) 1157.
[49] T. H. Boyer, Phys. Rev. **174**, (1968) 1764.
[50] K. A. Milton, Ann. Phys. **127**, (1980) 49.
[51] L. L. DeRaad, Jr. and K. A. Milton, Ann. Phys. **136**, (1981) 229.
[52] See, for example, E. M. Lifshitz, Sov. Phys. JETP **2**, (1956) 73.
[53] J. N. Israelachvili and D. Tabor, Proc. Roy. Soc. A **331**, (1972) 19.

*Starred documents attached to final report.

Measurement of multiple-electron emission in single field-emission events

M. A. Piestrup[a)]
Adelphi Technology, Inc., 2181 Park Boulevard, Palo Alto, California 94306

H. E. Puthoff
Institute for Advanced Studies at Austin, 4030 Braker Lane West, Suite 300, Austin, Texas 78759

P. J. Ebert[b)]
NOLASCO-Science Consultants, 1748 Applewood Road, Baton Rouge, Louisiana 70808

(Received 22 April 1997; accepted for publication 2 September 1997)

Thermal and field electron emission from a modified electron microscope W source were measured with an energy-dispersive counting system. Thermal-emission spectra were consistent with random emission of single electrons, while field-emission spectra were consistent with multiple-electron emission in random events. As many as 11 electrons were detected in isolated random field-emission events. © *1997 American Institute of Physics.* [S0021-8979(97)06023-4]

Most measurements of electron field emission (FE) are made with retarding field spectrometers and current measuring devices. It is impossible to determine how many electrons are emitted in a single FE event with these instruments. Herrmann and, later, Gazier first looked at individual events using energy-dispersive detectors.[1,2] For example, Gazier measured FE from W, W(Th), Pt, and Cu with an energy-dispersive Si(Li) spectrometer. Gazier's pulse height spectra, which indicated simultaneous arrival of as many as six electrons, were not consistent with random emission of single electrons.[2] Fursei and co-workers have carried out numerous experiments to measure FE electron statistics under a variety of experimental conditions, and have published extensively on this subject since 1975.[3–14] Their first results indicated multiple emission from W and Si.[3] However, in an experiment to measure FE from various facets of a clean W single crystal and at high vacuums, only single electron emission was observed.[5] In a 1991 paper that reviewed much of the work of Fursei and his colleagues, Fursei supposed that Gazier's multiple emission peaks were a result of parasitic secondary electron emission from the intermediate electrodes, and he concluded on the basis of many experiments that FE has a single particle character.[14]

Prompted by an unpublished experiment carried out by one of us (P.J.E.) at the Lawrence Livermore National Laboratory (LLNL) which supported Gazier's results,[15] James and co-workers undertook similar experiments with a thin-window proportional counter.[16–18] Their results also supported Gazier's experiment. Some experimental results are listed in Table I. Secondary electron emission caused by back-streaming ions impacting the cathode was judged not to be a cause of the multiple electron peaks.[15] We are not aware of any theoretical treatment of this phenomenon.

This article is a report of energy dispersive measurements of thermal emission (TE) and FE from single, isolated W tips. The experiments were undertaken in an attempt to clarify a rather confusing experimental situation and to identify the source of multiple-electron emission. A Siemens Elmiskop II transmission electron microscope was modified for this purpose. The electron source was standard, a commercially available W point filament that could be heated to 2800 K. Thus, the filament could be either a TE or FE source. It was positioned in the high field acceleration region of the microscope, through the cathode's aperture. There were no intermediate electrodes between the tip and the anode, which was held at ground potential. All beam optical components such as apertures and magnetic lenses were downstream of the anode. To center the beam on the axis of the microscope, the tip could be shifted in relation to the anode in two normal directions without breaking vacuum. The microscope, operated at 50 kV, was evacuated with an oil-diffusion pump. Typical operating pressure was 5×10^{-5} Torr or below. The microscope column had to be extended to accommodate a 25 mm^2 Si surface barrier detector that could be translated 100 mm along a horizontal axis. The detector was 595 mm from the tip, and was collimated with a 3 mm diameter iris to reduce the active detection area and to improve spatial resolution. The dimensions of the electron beam were controlled with the magnetic lens, and could be viewed with a retractable phosphorescent screen located 23 mm upstream of the detector. Charge pulses from the detector were processed in a counting system consisting of a preamplifier, a main amplifier, a multichannel analyzer, and a count rate meter. Amplified pulses ($\sim3\times10^{-6}$ s) were also monitored with an oscilloscope.

Because the spectra reported herein have unusual characteristics (up to 11 electrons arriving simultaneously), it is important to briefly consider the characteristics of our counting system. A count is a pulse that is registered in response to the deposition of energy in the detector. The detector is energy dispersive and linear, that is, the amplitude of the charge pulse generated in it is directly proportional to the energy deposited by the electron(s). Also, there is a fixed minimum time interval that separates two events such that they are recorded as separate pulses. During this interval, the system is "dead." Two electrons arriving during the dead time are recorded as a sum pulse, that is, a single pulse with twice the energy. We were concerned that the counting sys-

[a)]Electronic-mail: melpie@ix.netcom.com
[b)]Electronic-mail: pjebert@sprintmail.com

 0021-8979/97/82(11)/5862/3/$10.00

TABLE I. Compilation of experimental results.

Experimenters	T_c (kV)	Z	N[a]	n[b]	P (Torr)/T (K)	Detector comments
Herrmann[c]	15	W	1	1	10^{-6}/300	Proportional ctr.
Gazier[d]	40	W(Th)	5	1.3	10^{-6}/300	Cooled Si(Li)
Gazier	40	W	5	1.5	10^{-6}/300	Cooled Si(Li)
Gazier	40	Pt	6	1.5	10^{-6}/300	Cooled Si(Li)
Gazier	40	Cu	3	1.24	10^{-6}/300	Cooled Si(Li) low count rate
Fursei[e]	12	Si	4	1.41	10^{-9}/300	Si-surface barrier
Fursei[f]	12	W	2	1.03	10^{-9}/300	Si-surface barrier
Fursei[g]	17	W	1	1	10^{-10} 77–1000 K	Si-surface barrier; many facets of clean W single crystal
Fursei[h]	10	W	1	1	10^{-9}	Si-surface barrier; high current, $\Delta t = 10^{-10}$ s
Fursei[i]	20	Ceramic $YBa_2Cu_3O_{7-\delta}$	4	1.1	10^{-9} 4.2 K	Si-surface barrier, $B = 1$ T
Ebert[j]	30	W	6	1.7	10^{-4}/300	Proportional ctr.
Ebert	40	W	6	1.4	10^{-4}/300	Proportional ctr.
Ebert	40	W	8	1.5	10^{-6}/300	Cooled Si(Li) $\Delta E \sim 1$ keV
James[k]	9–30	W	6	1.4	10^{-6}/300	75 μm diam prop. ctr.
This work	50	W	11	1.6	10^{-5}/300	Si-surface barrier

[a]Note that N = number of multiple electron peaks in the measured spectrum.
[b]Note that n = average number of electrons detected per count in the measured spectrum.
[c]Reference 1.
[d]Reference 2.
[e]Reference 3.
[f]Reference 4.
[g]Reference 5.
[h]References 10 and 11.
[i]Reference 9.
[j]Reference 15.
[k]References 16–18.

tem might have been overwhelmed by the high rates at which data were accumulated, thereby giving rise to an inordinately large number of sum pulses.

Let the system resolving time be t, and the count rate for random emission of single electrons be r. Then the probability of detecting n electrons within t is given by

$$P_n(t) = (2rt)^n/n! \tag{1}$$

and $R_e(n)$, the expected ratio of counts of n electrons to single electron counts is

$$R_e(n) = P_n/P_1 = (2rt)^{n-1}/n! \tag{2}$$

Values of $R_e(n)$ for $n \leq 6$ are given in Table II for system resolving time of 3×10^{-6} and two vastly different count rates (15 and 16 500 counts/s) for which electron energy spectra were accumulated. Count rates were erratic and not controllable over the long term; however, count rates were monitored for stability during data collection. Figure 1 shows spectra acquired with the cathode at room temperature. The 16 500 counts/s spectrum was taken over a 15 min period; the 15 counts/s spectrum was taken over 4.75 h. The lowest energy peak is at 50 keV, and higher energy peaks are at integral multiples of the acceleration voltage. Peaks are ob-

TABLE II. Expected and measured peak ratios.

Peak number n	Energy (keV)	15 Counts/s		16 500 Counts/s	
		$R_e(n)$	$R_m(n)$	$R_e(n)$	$R_m(n)$
1	50	1	1	1	1
2	100	5.0×10^{-5}	3.0×10^{-1}	5.0×10^{-2}	3.5×10^{-1}
3	150	1.4×10^{-9}	1.4×10^{-1}	1.6×10^{-3}	1.2×10^{-1}
4	200	3.0×10^{-14}	7.2×10^{-2}	4.0×10^{-5}	5.3×10^{-2}
5	250	5.5×10^{-19}	4.0×10^{-2}	8.0×10^{-7}	2.0×10^{-2}
6	300	8.2×10^{-24}	2.2×10^{-2}	1.3×10^{-8}	8.1×10^{-3}

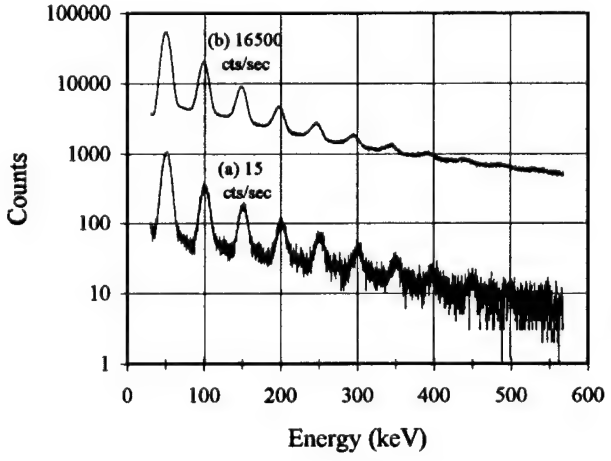

FIG. 1. Pulse height spectra taken from the W filament at room temperature but at different rates: 16 500 counts/s and 15 counts/s.

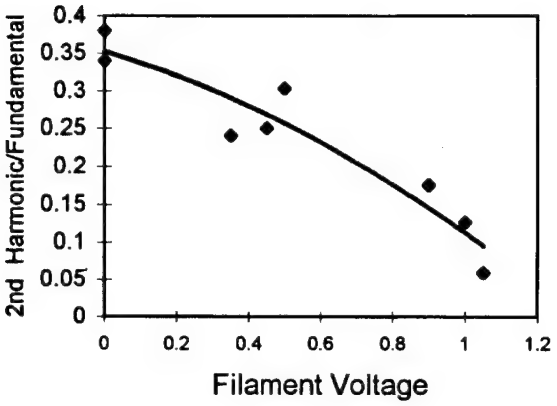

FIG. 2. Ratio of multiple counts to single counts vs filament voltage. Total emission increased with increasing voltage. Thermal emission overwhelmed the counting system with more than 1.1 V applied to the filament.

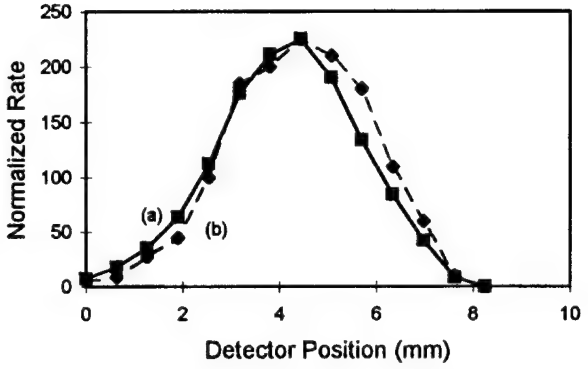

FIG. 3. The normalized rate of electron counts vs detector position for the cases of (a) thermal emission (TE) by counting single emission peaks and (b) field emission (FE) from harmonics above the fundamental, both originating from a W point filament. A 3 mm diam iris was used in measuring the FE and TE intensity profiles.

servable out to 550 keV, but the acceleration voltage was only 50 kV. The two spectra are very much like those obtained by Gazier,[2] Ebert,[15] and James.[16–18] Note, that in the high count rate spectrum, the peaks are shifted to slightly lower energy and the peak energy resolution is poorer, suggesting that the counting system was well behaved and operating properly. Also note that if the multiple energy peaks resulted from counting random single emission events in coincidence, then $R_m(n)$, the ratio of counts of n electrons to counts of a single electron would also be given by Eq. (2).

Expected values $R_e(n)$ are compared with measured values $R_m(n)$ in Table II. These were obtained by adding counts in each peak and subtracting the monotonically decreasing background. The measured values are orders of magnitude greater than the corresponding expected values. The value $R_m(2)$ at 16 500 counts/s is higher than the corresponding value for 15 counts/s. This is consistent with a higher number of random coincidences at the higher count rate. The differences in $R_m(n)$ for the other harmonics are smaller and are within the experimental errors for these ratios. Also, the average number of electrons detected per event was 1.7 ± 0.1 at 15 counts/s and 1.6 ± 0.1 at 16 500 counts/s. Therefore the multiple energy peaks or sum peaks must be from simultaneous emission of more than a single electron.

The FE rate could be overwhelmed by increasing the filament current, as can be seen in Fig. 2, which plots the ratio R_m $(n \geqslant 2)$ as a function of filament voltage. At 1.1 V, the emission is 95% thermal.

The electron beam was scanned to demonstrate that the source of multiple-electron emission was the tungsten tip. First, the TE electron source was imaged on the phosphorescent screen, and its position and size checked. The detector (3 mm diam) was then translated through the beam and the beam profile measured. Next, the filament current was turned off, the count rate meter's discriminator was raised to count pulses that were double energy and higher, and the beam profile of double energy and higher FE pulses was measured. The two profiles were virtually identical, as is evident in Fig. 3. The same result was obtained in a second scanning experiment with smaller irises and no magnetic focusing. In these scans, the profiles were wider, but overlaid each other. Thus the TE and FE sources were at the same location; multiple electron emission spectra were not a result of parasitic secondary electron emission from intermediate electrodes or other surfaces. Therefore, the multiple energy counts recorded must be regarded as detection of integral numbers of FE electrons that originated at the W tip and were detected within the resolving time of the counting system.

It should be noted that the major feature that distinguished experiments that routinely detected multiple emission from those which did not is that an electromagnet focused electrons that were emitted by the source. Another feature is that the vacuums were much poorer than in many of Fursei's experiments.

This research was sponsored by the United States Air Force Office of Scientific Research, Bolling AFB, DC.

[1] M. Hermman, Z. Phys. **184**, 354 (1965).
[2] C. Gazier, Phys. Lett. **35A**, 243 (1971).
[3] G. N. Fursei, M. M. Mokhasne, N. V. Egorov, V. S. Ponomarev, and V. N. Shchemelev, Sov. Phys. Solid State **18**, 368 (1976). The name "Fursei" is also spelled "Fursey" in some recent publications. Except for the references, we use the name as originally translated from the Russian.
[4] M. M. Mokhasne, V. S. Ponomarev, N. V. Egorov, G. N. Fursei, and V. N. Shchemelev, Instrum. Exp. Tech. **19**, 496 (1976).
[5] G. N. Fursei, N. V. Egorov, and A. V. Kocheryzhenkov, Sov. Tech. Phys. Lett. **7**, 343 (1981).
[6] N. P. Afanas'eva, N. V. Egorov, A. V. Kocheryzhenkov, and G. N. Fursei, Instrum. Exp. Tech. **25**, 1204 (1982).
[7] A. V. Kocheryzhenkov, V. I. Maslov, and G. N. Fursei, Sov. Phys. Solid State **29**, 1421 (1987).
[8] V. I. Maslov, G. N. Fursei, A. V. Kocheryzhenkov, and N. P. Afanas'eva, Instrum. Exp. Tech. **30**, 1162 (1987).
[9] G. N. Fursei, A. V. Kocheryzhenkov, V. I. Maslov, and A. P. Smirnov, Sov. Tech. Phys. Lett. **14**, 804 (1989).
[10] V. I. Maslov, G. N. Fursei, and A. V. Kocheryzhenkov, Sov. Tech. Phys. Lett. **34**, 1192 (1989).
[11] V. I. Maslov, G. N. Fursey, and A. V. Kocheryzhenkov, J. Phys. (France) **50**, C8-113 (1989).
[12] G. N. Fursei, A. V. Kocheryzhenkov, V. I. Maslov, A. L. Shmaev, and L. N. Borisov, Instrum. Exp. Tech. **33**, 152 (1990).
[13] V. I. Maslov, G. N. Fursei, and A. V. Kocheryzhenkov, Instrum. Exp. Tech. **33**, 395 (1990).
[14] G. N. Fursey, A. V. Kocheryzhenkov, and V. I. Maslov, Surf. Sci. **246**, 365 (1991).
[15] P. J. Ebert (unpublished).
[16] F. J. James, LLNL Contract Report, September 1993 (unpublished).
[17] F. James, P. Ebert, T. Miller, K. Wansley, and T. Terry, Bull. Am. Phys. Soc. **38**, 2174 (1993).
[18] F. James, Bull. Am. Phys. Soc. **40**, 952 (1995).

Publisher's Proof: to be published May/June 1998

Correlated Emission of Electrons

M. A. Piestrup
Adelphi Technology, Inc., 2181 Park Blvd., Palo Alto, California 94306

H. E. Puthoff
Institute for Advanced Studies at Austin, 4030 Braker Lane West, Suite 300, Austin, Texas 78759

P. J. Ebert
NOLASCO Science Consultants, 1748 Applewood Road, Baton Rouge, Louisiana 70808

We have studied the harmonic content of current generated by a single-point field emitter to determine if field emission electrons are correlated. We used a Si surface barrier particle detector to measure electron energy spectra at dramatically differing counting rates. Harmonic content was unusually high, with an average number of electrons per count of 1.6 for high (16,500 events/sec) and 1.7 for low (15 events/sec) count rates. This high harmonic content cannot be attributed to the counting system response, but must be considered as true events in which several electrons are emitted simultaneously and arrive within the resolution time of the detector and its electronics (~3 μsec). We also investigated possible spatial coherence by measuring the dependence of energy spectra on the area of the electron beam, whose size relative to that of the detector was varied using (1) a cylindrical magnet to increase beam diameter and (2) irises to reduce detector diameter. The harmonic content was larger than what one would expect if the spatial distribution of the electrons was entirely random, but not large enough to indicate that there is any attactive force between the simulateously emitted electrons that would overcome Coulomb repulsion.

Key Words: field emission, charge clustering, multiple electrons, anode spots.

1. Introduction

Electron field emission has been studied under a variety of experimental conditions. For the purposes of this discussion, we consider three levels of electron beam current: (a) low current where isolated emission events can be counted[1-19]; (b) moderate current where sporadic, noisy pulses are recorded with current measuring devices[20, 21]; (c) high current where plasma effects generally dominate[22-30] and plasma diagnostic techniques are employed. It has not been generally recognized that seemingly unrelated observations of electron clustering in the three current regimes may be governed by similar or related physics.

At low current, researchers were able to measure electron energy and hence spatial and temporal correlation between charges in isolated particle counting events. Herrmann and, later, Gazier first studied individual events using energy-dispersive detectors [1,2]. Gazier detected field-emitted multiple-electron events (2 to 5 electrons) originating in a region of less than 1 mm. Fursey has carried out extensive research in this area over the past two decades [3-14]. He and his colleagues have evaluated the effects of the field emitter temperature, emitter material composition and orientation, and pressure. They also investigated the influence of adsorption of residual gases on the harmonic content of the field emission, since this seemed important in the explanation of Gazier's experiments. Fursey's early results indicated field emission was of single electron character only (no harmonics). This lead to the conclusion that Gazier's results were artifacts connected with parasitic secondary emission from the intermediate electrodes [14]. Prompted by an unpublished low-current experiment that supported Gazier's results [15] which was carried out by one of us at the Lawrence Livermore National Laboratory (LLNL), James and coworkers undertook similar experiments with a thin-window proportional counter [16-18]. Their results also supported Gazier's experiment, as do the results reported herein and in [19]. A summary of low-current experimental results is tabulated in [19].

In the moderate current regime, emission current from field emitters (Spindt cathodes) is sporadic[20]. Single molybdenum tips exhibit burst (popcorn or telegraph) noise that consists of sequences of bi-stable current pulses of specific amplitude, but with random lengths and random intervals between pulses. These current pulses are separated by quiescent periods, which may be of the order of tens to hundreds of seconds. Current measurements of single Spindt cathodes are in the 10^{-6} to 10^{-8} A range. The burst noise sequences themselves may last from milliseconds to hours. As the resolving time is made shorter, burst current pulses are seen to consist of pulses of similar character, with a limiting pulse length on the order of milliseconds according to Kirton and Urens [21].

In the high current regime, experiments by Shoulders have indicated that high-density spherical charge clusters are possible [22-24]. His work in this area was limited to techniques that are more heuristic than would be desirable for proof of their existence. Shoulders' evidence that field emitted electrons were clustered is both passive (the form of craters on anode surfaces) and active (photographs with a high speed camera). Experiments and modeling which used more conventional plasma physics to describe the presence of spherical impact craters were reported by Schwirzke et al. [29] and Wright [30]. They observed circular cratering of both anode and cathode, and their explanation for this emission is quite different from Shoulders' [22]. Theo-

retical discussions of electron clustering were published by Beckmann, Aspden [25,26] and by Ziolkowski and Tippett[27,28]. Given the nature of Coulomb repulsion, it is difficult at first glance to understand spatial clustering of high current electrons without charge neutralization by trapped ions or image charges. However, as shown by these researchers [25-28] and by two of us [31] other mechanisms for clustering are possible.

A survey of the literature suggests that researchers in these three different current regimes were not generally aware of each other's work. To clarify some of these issues, experiments in the low current regime reported here and in [19] were undertaken with an energy dispersive Si surface barrier detector to determine both the temporal and spatial characteristics of thermal and field emission from single, isolated W tips.

2. Experiment

2.1. Apparatus

We utilized a modified transmission electron microscope to observe the energy spectra from a point tungsten filament. The experimental apparatus is shown schematically in Fig. 1. The electron source was standard, a commercially available W point filament that could be heated to 2800°K. Thus, the filament could be either a thermal emission (TE) or field emission (FE) source. The tip was positioned in the high field acceleration region of the microscope, through the cathode's aperture. There were no intermediate electrodes between the tip and the anode which was held at ground potential. All beam optical components such as apertures and magnetic lenses were downstream of the anode. To center the beam on the axis of the microscope, the tip could be shifted in relation to the anode in two normal directions without breaking vacuum. The microscope was operated at 50 kV, and was evacuated with an oil-diffusion pump. Operating pressure was 5 x 10^{-5} Torr or below. The microscope column had to be extended to accommodate a 25 mm^2 Si surface barrier detector that could be translated 100 mm along a horizontal axis. The detector was 595 mm from the tip, and was collimated with a 3-mm diameter iris to reduce the active detection area and to improve spatial resolution. The dimensions of the electron beam were controlled with the magnetic lens, and could be viewed with a retractable phosphorescent screen located 25 cm upstream of the detector. Charge pulses from the detector were processed in a counting system (see Fig. 2) consisting of a preamplifier, a main amplifier, a multichannel analyzer and a count rate meter. Amplified pulses (~ 3 x 10^{-6} sec) were also monitored with an oscilloscope.

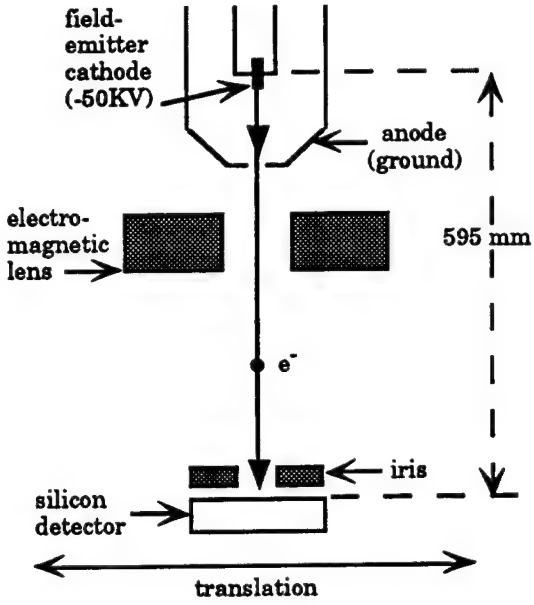

Figure 1. The apparatus used to study charge correlation.

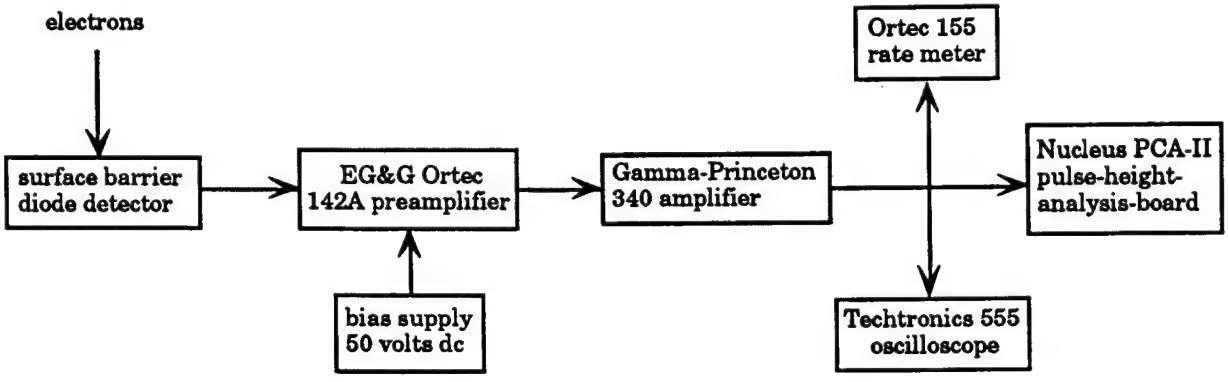

Figure 2. Block diagram of the electronics for pulse height analysis of the electron energy spectrum [29].

2.2 Counting System Behavior

Because the spectra reported herein have unusual characteristics (up to 11 electrons arriving simultaneously), it is important to briefly consider the characteristics of our counting system[32]. A count is a pulse that is registered in response to the deposition of energy in the detector. The detector is energy dispersive and linear, that is, the amplitude of the charge pulse generated in it is

directly proportional to the energy deposited by the electron(s). Also, there is a fixed minimum time interval that separates two events such that they are recorded as separate pulses. During this interval, the system is "dead." Two electrons arriving during the "dead" time are recorded as a sum pulse, a single pulse with twice the energy. We were concerned that the counting system might have been overwhelmed by the high rates at which data were accumulated, thereby giving rise to an inordinately large number of sum pulses.Let the system resolving time be t, and the count rate for random emission of single electrons be r, then the probability of detecting n electrons within t is given by[32]

$$P_n(t) = (2rt)^n / n! \tag{1}$$

and $R_e(n)$, the expected ratio of counts of n electrons to single electron counts is

$$R_e(n) = (2rt)^{n-1} / n! \tag{2}$$

Values of $R_e(n)$ are given in Table 1 for count rates of 15 and 16,500 counts/sec, and system resolving time of 3×10^{-6} sec.

3. Experimental Results

3.1. Pulse Height Spectra

Electron-energy spectra were accumulated under several experimental conditions. The count rates were erratic and not controllable over the long term; however, count rate was monitored for stability during data collection. Fig. 3 shows spectra acquired at two vastly different count rates with the cathode at room temperature. The spectrum in 3(a) was taken over a 15 minute period at a count rate of 16,560 counts/sec, while spectrum 3(b) was taken over a 4.75 hour period at a count rate of 15 counts/sec. The lowest energy peak is at 50 keV, and higher energy peaks are at integral multiples of the acceleration voltage. Peaks are observable out to 550 keV, but the acceleration voltage was only 50 keV.

The two spectra are similar, and are very much like those obtained by Gazier,[2] Ebert[15] and James, et al.[16-18] Note that in the high count rate spectrum, the gain is shifted to slightly lower energy and peak energy resolution is poorer, suggesting that the counting system was well behaved and was operating properly. Also note that if the multiple energy peaks resulted from counting random single electron emission events in coincidence, then R(n), the ratio of counts of n elections to counts of a single electron would also be given by equation (2).

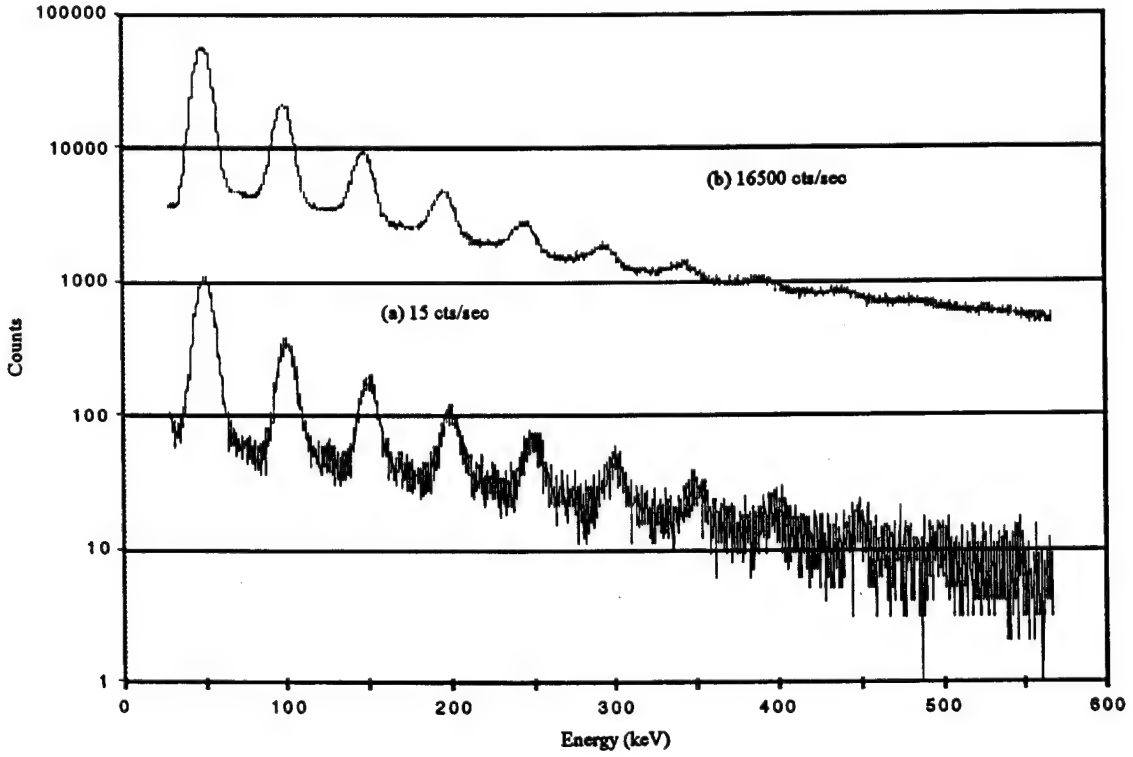

Figure 3. Pulse height spectra taken from the same field emitter but at different rates: 16,500 counts/sec and 15 counts/sec (from [19]).

Measured values $R_m(n)$ are compared with expected values $R_e(n)$ in Table 1. These were obtained by adding counts in each peak and subtracting the monotonically decreasing background. The measured values are orders of magnitude greater than those expected. The value $R_m(2)$ at 16500 counts/sec is higher than the corresponding value for 15 counts/sec. This is consistent with a higher number of random coincidences at the higher count rate. The differences for the other harmonics are smaller and are within the experimental errors for these ratios. Also, the average number of electrons detected per event was 1.7 ± 0.1 at 15

counts/sec and 1.6 ± 0.1 at 16500 counts/sec. Therefore the multiple energy peaks must be from simultaneous emission of more than a single electron.

Table 1. Expected and Measured Peak Ratios

peak	energy	15 counts/sec.		16500 counts / sec.	
no., n	keV	$R_e(n)$	$R_m(n)$	$R_e(n)$	$R_m(n)$
1	50	1	1	1	1
2	100	5.0×10^{-5}	3.0×10^{-1}	5.0×10^{-2}	3.5×10^{-1}
3	150	1.4×10^{-9}	1.4×10^{-1}	1.6×10^{-3}	1.2×10^{-1}
4	200	3.0×10^{-14}	7.2×10^{-2}	4.0×10^{-5}	5.3×10^{-2}
5	250	5.5×10^{-19}	4.0×10^{-2}	8.0×10^{-7}	2.0×10^{-2}
6	300	8.2×10^{-24}	2.2×10^{-2}	1.3×10^{-8}	8.1×10^{-3}

3.2. Electron Emission Source

The microscope's magnetic objective lens was used to demonstrate that the source of multiple electron emission (the FE source) was the tungsten tip. First, with the filament heated, the TE electron source was imaged on the phosphorescent screen, and its position and size checked. The detector was then translated through the beam and the beam profile measured. Next, the filament current was turned off, the count rate meter's discriminator was raised to count pulses that were double energy and higher, and the beam profile of double energy and higher pulses was measured. The two profiles were virtually identical[19]. To obtain higher spatial resolution, the iris sizes were reduced. The diameter of the iris for measuring TE was ~ 100 μm, while that for FE was 2 mm. The electromagnet was turned off to let the electron beam expand. With the filament off, the beam profile of double energy counts was measured (using counts from the pulse height analysis spectrum) and compared with that of the TE profile (using the count rate meter). As is evident in Fig. 4, the normalized profiles for the TE and FE distributions are nearly the same. The difference in resolution of the FE and TE distributions was due to the differing iris sizes. Thus the TE and FE sources were at the same location.

3.3. Effects of field emitter temperature

The emission rate also depended on the temperature of the field emitter. In this experiment, we utilized the fact that the tungsten field emitter could also be operated as a thermal emitter of electrons. We found that the rate of emission increases with increased temperature; however, the ratio of harmonics to the fundamental decreases as the emitter temperature increases. The FE rate could be overwhelmed by increasing the filament current, as can be seen in Fig. 5, which plots the ratio $R_m(2)$ as a function of filament voltage. The beam is nearly 100% thermal at 1.1 volts across the filament. The rate of emission over the 1.1 volt range varied from a few events/sec up to 10^5 events/sec (the limit of the detector electronics resolution). Thus although the relative harmonic content decreased, the overall rate of harmonic generation increased with increasing temperature.

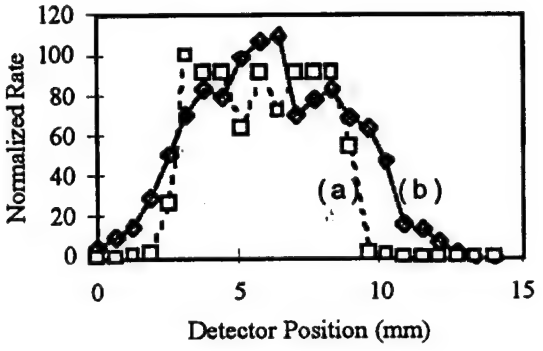

Figure 4. The normalized count rate of electrons for the cases of (a) thermal emission and (b) the field emission from harmonics above the fundamental both originating from a W point filament. A 2-mm iris was used to measure the FE rate ($\geq 2^{nd}$ harmonic) and a 100 μm iris was used to measure the TE rate.

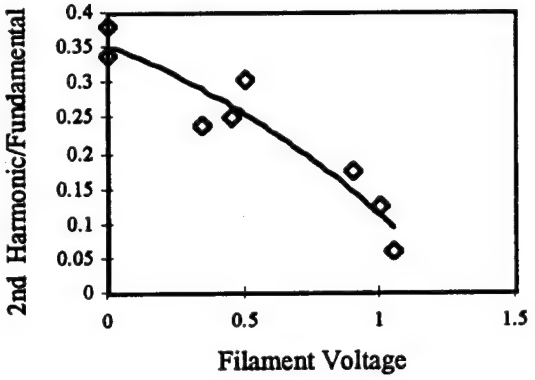

Figure 5. Harmonic content as a function of filament voltage (from [19]).

3.4. Effects of Detector Aperture Size

In our first experiment to explore the possibility that the electrons are spatially correlated, we increased the area of the electron beam so that it was much larger than the area of the Si detector aperture. The assumption was made that loss of higher harmonics would occur if the electrons were not spatially bound. If this was indeed the case, the electrons would have independent trajectories and would result in fewer counts in the harmonics relative to the fundamental. If the electrons are strongly correlated spatially, they will stay together with the same trajectory. Thus the energy spectrum of the increased area beam should still have a high harmonic content.

By simple calculation we can estimate the harmonic content of the beam. Assuming that the electrons stay completely correlated, the expanded electron beam would have the same harmonic content as in the case where the entire beam is focused on

the detector. Measurements for the focused case showed that the ratio of the 2nd harmonic to the fundamental was 0.38. Thus, if the electrons remained totally spatially coherent, expanding the area of the beam at the detector would only reduce the rate of detection, not the harmonic content, and the ratio should remain 0.38. On the other hand, if the electrons were moving totally independently of one another, then the harmonic content would be reduced by the ratio of the area of the detector to that of the expanded area.

The pulse height spectra for the cases where the beam is focused onto the detector and where the beam's spot size is increased to 5 cm and 12 cm diameter are shown in Fig. 6. Both the rate and the harmonic content are seen to drop with increasing beam area. The measured ratio of the second harmonic to fundamental was 0.38 for the case where the electron beam was focused into the detector. Since the active area of the detector was 25 mm² (5.6 mm diameter), while the expanded electron beam at the detector was 1962 mm² (5 cm diameter), we should expect the 2nd harmonic/fundamental to be (25/1962) x 0.38 = 0.005 for the case of spatially uncorrelated electrons. For the 5 cm beam, the measured ratio of the 2nd harmonic to the fundamental was 0.08, a factor of 4.7 less than that of the focused case, but a factor of 16 higher than the incoherent case. Thus, the electrons show partial spatial coherence even after traveling a distance of 59.5 cm from the field emitter to the detector. The measured ratios of the 2nd harmonic/fundamental for the 5 cm and a 12 cm diameter spots are given in Table 2.

Table 2. Harmonic Ratios for Different Focus Settings

beam size at the detector	measured ratio second harmonic +fundamental	expected ratio assuming no spatial coherence
focused	0.38	0.38
5 cm	0.08	0.005
12 cm	0.008	0.0008

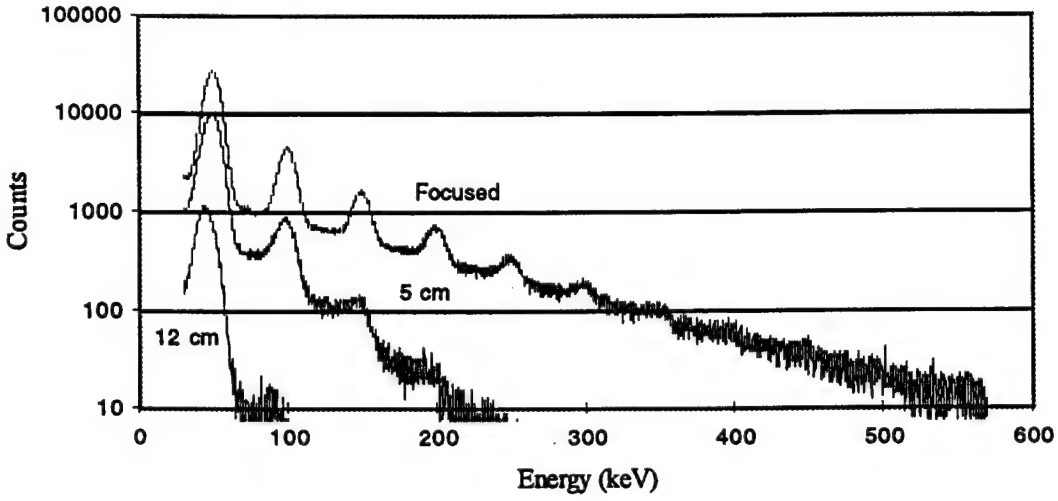

Figure 6. Pulse height spectrum from a tungsten field emitter for the cases of focused, 5 cm and 12 cm spot sizes at the detector. Detector active area is 25 mm^2.

3.5. Electron beam size reduction

To see if the magnetic focusing contributed to the increased randomization of the electron beam, we utilized the apertures (1.3 mm and 0.65 mm diameter irises) of the cylindrical magnet (with magnet off) to define the size of the electron beam. The electron beam was allowed to naturally expand as it traveled to the detector. The measured size of the electron beam at the detector was 1 cm. The irises could be placed 27.8 cm from the field emitters and 48.4 cm from the detector. In this experiment the detector was 762 mm from the source. We estimate the spot size of the beam to be 5 mm at the iris. As discussed above, limiting the size of the electron beam should not reduce the harmonic content if the electrons are highly spatially correlated. The results are shown in Fig. 7, where we compare three spectra, one with no aperture, one with 1.3 mm and one with 0.65 mm. The expected and the measured 2nd harmonic/fundamental ratios are given in Table 3. The expected value for no spatial coherence are calculated by assuming that the harmonic content is reduced by the ratio area of the irises to that of the area of the electron beam. Again the measured values show a degree of spatial correlation. For both irises, the measured ratio was a factor of 10 or more higher than the expected value if the electrons were uncorrelated.

Table 3. Harmonic Ratios for Different Iris Sizes

iris size	measured ratio second harmonic +fundamental	expected ratio assuming no spatial coherence
focused	0.38	0.38
1.3 mm	0.26	0.025
0.65 mm	0.09	0.006

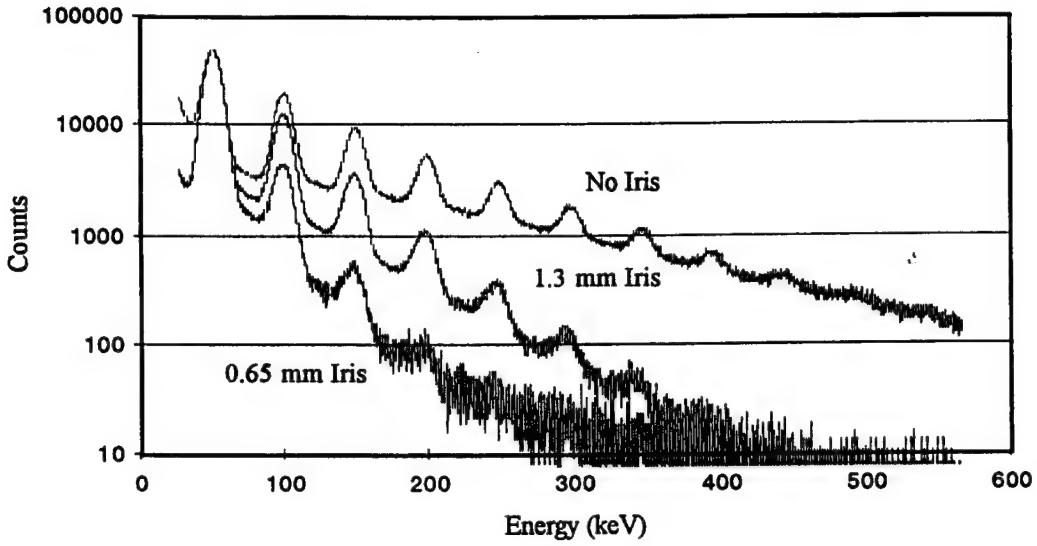

Figure 7. Pulse height spectrum from a tungsten field emitter for the cases of no iris and 1.3 mm, and 0.65 mm irises.

4. Discussion

We have observed the pulse height spectrum out to 600 keV (>10 electrons/bunch). Harmonic content does not vary appreciably with different tungsten field emitters. Each group or bunch of electrons is emitted simultaneously (within the resolving time of the detection system) from a highly localized point on the field emitter.

The rate of generation of the second harmonic can be used to map the spatial distribution of the cluster spectrum. Heating the field emitter results in an increase in total emission rate, but a decrease in the relative harmonic content of the energy spectrum. This indirectly shows that the multiple emission is coming directly from the field emitter and not from parasitic secondary emission from electrons striking the anode aperture.

In addition, our measurements have shown that there is harmonic content to electron beams whose diameters are larger than that of the detector aperture, thus showing that the electrons remained correlated over a large distance from the field emitter.

However, this effect is not strong and cannot be said to show that there is an attractive force between the field emitted electrons.

Since there is no attractive force to keep the electrons together, the use of a cylindrical magnet to collect and focus electrons onto the detector was important to demonstrating temporal correlation. The magnet functions to keep all the simultaneously emitted electrons together so that they will be count ed as a multiple electron pulse. Indeed, the experiments of Fursey et al. [3-14] do not appear to use focusing and this may be the reason their results have fewer (and in some cases, no) multiple counts. It should be noted that another distinguishing feature of experiments that routinely detected multiple emission was that the vacuums were much poorer than in many of Fursei's experiments.

In summary, laboratory observation of high-density filamentation or clustering of electronic charge has motivated an investigation into potential cohesive mechanisms whereby repulsive Coulomb forces can be overcome by some form of compensatory attractive force. A class of models which invoke the possibility of charge confinement by van der Waals-type forces was suggested by Casimir. The resulting analysis [31] and the experimental results presented here indicate that confinement of small numbers of electrons by the van der Waals mechanism cannot be achieved under experimental conditions considered herein. However, as shown in [31], large numbers can be clustered by the van der Waals force.

Acknowledgment

This research was sponsored by the United States Air Force Office of Scientific Research, Bolling AFB DC.

References

[1] M. Herrmann, "Investigation of different processes of multiple electron emission", (in German) Z. Phys. 184, 352-354 (1965)..

[2] C. Gazier, "Multiple-electron events from field emission", Phys. Letts. 35A , 243-244 (1971)..

[3] G.N. Fursei, M.M. Mokhasne, N.V. Egorov, V.S. Ponomarev, and V.N. Shchemelev, "Statistics of field-electron emission", Sov. Phys. Solid State 18, 368-369 (1976)..

[4] M.M. Mokhasne, V.S. Ponomarev, N.V. Egorov, G.N. Fursei, and V.N. Shchemelev, "A procedure for investigating the statistics of field emission", Instrum. Exp. Tech. (USA) 19, 496-498 (1976)..

[5] G.N. Fursei, N.V. Egorov and A.V. Kocheryzhenkov, "Field-emission statistics for various faces of a tungsten single crystal", Sov. Tech. Phys. Lett. 7, 343-345 (1981)..

[6] N.P. Afanas'eva, N.V. Egorov, A.V. Kocheryzhenkov and G.N. Fursei, "A method of examining the number of electrons produced

in an elementary act of field emission", Inst. Exp. Tech. (USA) 25, 1204-1206 (1982)..

[7] A.V. Kocheryzhenkov, V.I. Maslov and G.N. Fursei, "Statistics of field-electron emission from tungsten and niobium at helium temperatures", Sov. Phys. Solid State 29, 1421 (1987)..

[8] V.I. Maslov, G.N. Fursei, A.V. Kocheryzhenkov, and N.P. Afanas'eva, "Apparatus for study of statistics of field emission at low temperatures", Instrum. Exp. Tech. (USA) 30, 1162-1164 (1987)..

[9] G.N. Fursei, A.V. Kocheryzhenkov, V.I. Maslov and A.P. Smirnov, "Multiparticle tunneling during field emission from $YBa_2Cu_3O_{7-\delta}$", Sov. Tech. Phys. Lett. 14, 804-805 (1989)..

[10] V.I. Maslov, G.N. Fursei and A.V. Kocheryzhrnkov, "Statistics of field emission for tungsten over a wide range of current densities", Sov. Phys. Tech. Phys. 34, 1192-1194 (1989)..

[11] V.I. Maslov, G.N. Fursei and A.V. Kocheryzhenkov, "Investigations of the quantity of elementary acts of field emission with time resolution of 5 μs to 100 ps", J. de Physique 50 C8 supplement, C8-113 to C8-117 (1989)..

[12] I. Maslov, G.N. Fursey and A. V. Kocheryzhenkov, "Method for study of field emission statistics over a wide current-density range", Instruments and Experimental Techniques, 33, 395-399 (1990)..

[13] G.N. Fursey, A.V. Kocheryzhenkov and V.I. Maslov, "The quantity of elementary acts and the statistics of field emission", Surface Science 246, 365-372 (1991)..

[14] G.N. Fursey, A.V. Kocheryzhenkov, V.I. Maslov, A.L. Shamaev, and L.N. Borisov, "Apparatus for study of multiparticle acts of field emission at low temperatures", Instruments and Experimental Techniques, 33, 152-154 (1990)..

[15] P.J. Ebert, Unpublished experimental results (1970); excerpted from unpublished research proposal (1990)..

[16] F.J. James, LLNL contract report, September 1993. unpublished.

[17] F. James, P. Ebert, T. Miller, K. Wansley and T. Terry, "Production of multiple electron peaks from a tungsten electron gun in field emission mode", Bull. Am. Phys. Soc. 38, 2174 (Nov. 4-6, 1993)..

[18] F. James, "Time study of multiple electron peaks produced by a tungsten electron gun in field emission mode", Bull. Am. Phys. Soc. 40, 952 (1995)..

[19] M.A. Piestrup, H.E. Puthoff and P.J. Ebert, "Measurements of multiple-electron emission in single field-emission events," accepted for publication in J. Appl. Phys. Comm 82 (11). (1997)..

[20] C.A. Spindt, I. Brodie, L. Humphey, and E.R. Westerberg, "Physical Properties of thin field emission cathodes, with molybdenum cones", J. Appl. Phys. 47, 5248-5263 (1976)..

[21] M.J. Kirton and M.J. Urens, "Noise in solid state microstructures", Adv. in Phys. 38, 367-468 (1989)..

[22] K.R. Shoulders, EV: A Tale of Discovery (Jupiter Technologies, Austin, TX, 1985)..

[23] K.R. Shoulders, "Method of and apparatus for the production and manipulation of high density charge," U.S. Patent Number 5,054,046.

[24] K.R. Shoulders, "Circuits responsive to and controlled by charged particles," U.S. Patent Number 5,054,047.

[25] P. Beckmann, "Electron Clusters", Galilean Electrodynamics 1, 55-58 (1990)..

[26] H. Aspden, Correspondence, Galilean Electrodynamics 1 ,81 (1990)..

[27] R.W. Ziolkowski and M.K. Tippett, "Collective effect in an electron plasma system catalyzed by a localized electromagnetic wave", Phys. Rev. A 43, 3066-3072 (1991)..

[28] R.W. Ziolkowski, "Electromagnetic localized waves that counteract Coulomb repulsion to catalyze a collective electron-paxcket state", Phys. Rev. E 52, 5338-5343 (1995)..

[29] F. Schwirzke, M.P. Hallal, X.K. Maruyama, "Onset of Breakdown and formation of cathode spots", IEEE Trans. on Plasma Science, 21, 410-415 (1993)..

[30] C.M. Wright, "Time resolved measurements of light produced by onset of plasma formation on electrodes of fast pulsed high voltage diodes", thesis, Naval Postgraduate School, (Monterey, CA, Dec. 1994).

[31] H.E. Puthoff and M.A. Piestrup, "The Possibility of Charge Confinement by van der Waals-type-Casimer Forces," Submitted to Phys. Lett. B.

[32] G.F. Knoll, Radiation Detection and Measurement, 2nd Ed., (John Wiley & Sons, New York, 1989).

Charge Confinement by van der Waals/Casimir-Type Forces

H. E. Puthoff[1*] and M. A. Piestrup[2]

[1]Institute for Advanced Studies at Austin, 4030 Braker Lane W., Suite 300, Austin, Texas 78759-5329

[2]Adelphi Technology, Inc., 2181 Park Boulevard, Palo Alto, California 94306

Abstract

Laboratory observation of high-density filamentation or clustering of electronic charge suggests that under certain conditions strong coulomb repulsion can be overcome by cohesive forces as yet imprecisely defined. Following an early suggestion by Casimir, we investigate here the possibility that van der Waals/Casimir-type forces can lead to charge clustering of the type observed, and conclude that such forces may play a role in the generation of robust high-charge-density effects.

PACS: 79.70.+q, 52.80.Mg

Key Words: electron, charge clustering, Casimir force, van der Waals, zero-point energy

* puthoff@aol.com

I. Introduction

The formation of high-density, electronic-charge clusters has been reported to occur under certain precisely-defined laboratory conditions[1-3]. This phenomenon is of interest with regard to numerous potential applications, ranging from high-power microelectronic devices based on micro-arc discharge processes, to the containment of plasma for fusion purposes.[1]

Aside from the trivial case of electron charge neutralization by positive ions, mechanisms proposed in the literature for high-density charge confinement range from standard magnetic pinch models to exotic, soliton-like localized-wave (LW) solutions in plasma-EM wave interactions[5].

Another candidate mechanism that has yet to be fully explored with regard to charge confinement is provided by the short-range, attractive van der Waals and Casimir forces driven by vacuum-fluctuation phenomena. Such forces derive from the fact that the vacuum, rather than being the void of classical theory, is the seat of electromagnetic zero-point fluctuations (ZPF) of enormous energy density and radiation pressure. Theory predicts and experiments verify the existence of the van der Waals-type forces between closely-spaced metallic or dielectric boundaries, and between free charge distributions. One example is the Casimir force, the attractive, ZPF-induced quantum force between conducting parallel plates[6-9], recently measured with good precision[10]. Detailed analysis shows that the attractive force is due to a

---

[1] One application of current interest is that of small-scale accelerators in which positive gas ions, swept up by electron charge clusters in a collective acceleration process, are given an effective energy-gain boost $G \approx \left(m_p/m_e\right)\left(A/I\right)$, where m_p and m_e denote the proton and electron masses, and A and I are the atomic mass number and ionization charge number of the ion, respectively[4]. The energy gain results from the fact that N_i ions bound by coulomb force to an electronic charge cluster of N_e electrons, where $N_i << N_e$, arrive at an accelerating target anode with a velocity determined essentially by the charge-to-mass ratio of the electrons. As a result, KeV-level accelerating potentials can be used to generate MeV-level ion impacts, of use in, e.g., table-top nuclear experimentation.

partial shielding of the ZPF radiation pressure from the interior region of the plates, which results in the plates being pushed together[11].

As to the issue of charge confinement specifically, it was Casimir himself who first proposed that the ZPF-induced pressure forces might provide a mechanism for the confinement of charge in (semi-classical models of) elementary particles, a problem even more challenging than the laboratory one under consideration here[12]. To explore this concept in some detail here we examine, first, the lower limiting case of the van der Waals attraction between two isolated charges, and then the collective behavior involving multiple charge distributions of various geometries.

II. Two-Particle van der Waals force Interaction

The ZPF-induced van der Waals interaction between a pair of polarizable particles is given by [13-15]:

$$U_{vdw}(R) = \mathrm{Re}\left\{-\frac{\alpha^2\hbar c}{\pi}\int_0^\infty du\,\frac{u^4\omega_0^4}{(c^2u^2+\omega_0^2)^2}\,\frac{e^{-2uR}}{R^2}\left[1+\frac{2}{(uR)}+\frac{5}{(uR)^2}+\frac{6}{(uR)^3}+\frac{3}{(uR)^4}\right]\right\} \quad (1)$$

where $\alpha = q^2/4\pi\varepsilon_0 m\omega_0^2$ is the static polarizability of each particle, and $u = -ik = -i\omega/c$.

For a free particle (electron) $\omega_0 \to 0$, and the above can be simplified to

$$U_{vdw}(R) = -\frac{9}{4}\frac{\hbar c^3\Gamma^2}{\pi R^3}\int_0^\infty dx\left[\sin(2x)+\frac{2\cos(2x)}{x}-\frac{5\sin(2x)}{x^2}-\frac{6\cos(2x)}{x^3}+\frac{3\sin(2x)}{x^4}\right], \quad (2)$$

where x = kR and $\Gamma = q^2/6\pi\varepsilon_o mc^3$.

Term by term integration then leads to an expression of the form (with y = 2x)

$$U_{vdw}(R) = -\frac{9}{4}\frac{\hbar c^3 \Gamma^2}{\pi R^3}\left[\frac{1}{2}\int_0^\infty dy \sin y + \frac{2}{3}\right]. \qquad (3)$$

The final step in the evaluation of the integral is to realize that at some high frequency the free-electron response to the ZPF can be expected to drop off. Thus we can insert an integrating factor of the form $e^{-\lambda y}$ into the integrand in (3) and then let $\lambda \to 0$ after the calculation,

$$\lim_{\lambda \to 0} \int_0^\infty dy e^{-\lambda y} \sin y = \lim_{\lambda \to 0} Im \int_0^\infty dy e^{(-\lambda + i)y} = \lim_{\lambda \to 0}\left[-Im\frac{1}{-\lambda + i}\right] = 1, \qquad (4)$$

yielding for the final result

$$U_{vd\omega}(R) = -\frac{21}{8}\frac{\hbar c^3 \Gamma^2}{\pi R^3}. \qquad (5)$$

An excellent overview placing such calculations within a broad context of particle interactions is provided by Spruch[16].

We are now in a position to inquire as to the close-approach distance where, aside from other considerations, the repulsive coulomb force would be overcome by an attractive van der Waals force as calculated here. The total potential for the two can be written in the form

$$\frac{U(R)}{m_e c^2} = \frac{r_e}{R} - \frac{7}{6\pi}\left(\frac{\hbar/m_e c}{r_e}\right)\left(\frac{r_e}{R}\right)^3, \qquad (6)$$

where $(\hbar/m_e c)$ and r_e are, respectively, the Compton and classical electron radii. The total force F, given by $F = -dU(R)/dR$, would go to zero (forces would balance) at $R \sim 12.4\, r_e \sim 3.5 \times 10^{-14}$ m. Having completed this calculation, however, we recognize that we have exceeded the limits of applicability of such a simple model of van der Waals capture and confinement; e.g., confinement at such close spacing would be opposed by yet another "force," the so-called

"Schrödinger pressure." The Schrödinger pressure, about which more will be said in the following section, is a force that resists particle confinement due to the wave nature of matter that can be seen as deriving from a combination of the uncertainty and Pauli exclusion principles[17]. Balance of this force $\left(\approx \hbar^2/mR^3\right)$ by the van der Waals force cannot be achieved under realistic conditions, and so we must turn to the multiparticle case for such a possibility.

III. Multiparticle van der Waals/Casimir-Force Interaction

Early investigation by Casimir of vacuum-fluctuation-driven, multiparticle van der Waals interactions led to the realization that summation over the collective particle-particle interactions could be recast to advantage in terms of the restructuring of vacuum energy in response to the boundaries defined by the particle distributions[6]. This is because charge distributions which can respond to fields constitute boundaries which reconfigure those fields, vacuum ZPF fields included. The classic example is the Casimir effect mentioned in the Introduction. Conducting parallel plates exclude all but a finite number of modes in the interior spacing, with the consequence that the radiation pressure outward on the plates associated with the interior modes is less than the pressure inward due to the (essentially infinite in number) external modes. This yields a net radiation pressure which drives the plates together with a force per unit area given by[11]

$$\frac{F}{A} = -\frac{\pi^2}{240}\frac{\hbar c}{d^4}, \tag{7}$$

where d is the spacing between the plates.

With regard to the containment of high-density charge, originally of interest for the development of semiclassical models of elementary particles, Casimir suggested that a shell-like distribution of charge might partially shield vacuum fields from the interior of the shell with the result that net inward radiation pressure would compensate outwardly-directed coulomb forces to yield a stable configuration at small dimensions. Along these lines Casimir offered two models for consideration[12], one which assumes total shielding of interior fields up to a Compton-frequency cutoff for electron-ZPF field interactions, and a second in which interior fields associated with discrete states permitted by boundary conditions are assumed to exist, as in the parallel-plates example above. We examine both possibilities here.

IV. Casimir's Shell Model I

The plausibility of Casimir's first model (total shielding of interior fields up to some cutoff frequency) finds some support in recent work by one of the authors (H.P.). This work traces the source of ZPF fields to the quantum-fluctuation motion of charged particles distributed over cosmological space[18]; such fields could then in principle be shielded from an interior space by a sufficiently dense charge distribution.

With the spectral energy density of the ZPF fields given by

$$\rho(\omega)d\omega = \frac{\hbar\omega^3}{2\pi^2 c^3}d\omega, \tag{8}$$

integration over frequency from zero up to a cutoff frequency Ω_c for electron-ZPF interactions yields a vacuum energy density u_V effective in such interactions,

$$u_v = \int_0^{\Omega_c} \rho(\omega) d\omega = \frac{\hbar \Omega_c^4}{8\pi^2 c^3} \quad . \tag{9}$$

Now assume a spherical-shell distribution of N electrons on a shell of radius a. For the ZPF radiation pressure to compensate the electrons' coulomb stress, we require (1/3) $u_V = u_e$, or

$$\frac{1}{3}\frac{\hbar \Omega_c^4}{8\pi^2 c^3} = \frac{1}{2}\varepsilon_0 E^2 = \frac{N^2 \alpha \hbar c}{8\pi a^4}, \tag{10}$$

where here α is the fine structure constant, $\alpha = e^2/4\pi\varepsilon_0 \hbar c \approx 1/137.036$. This leads to an expression for the cutoff frequency,

$$\Omega_c = (3\pi\alpha)^{1/4} \sqrt{N} \left(\frac{c}{a}\right). \tag{11}$$

Alternatively, the above expression can be derived by equating the ZPF energy missing from the interior of the sphere to that stored in the coulomb field.

With regard to the cutoff frequency Ω_c for electron-ZPF interactions, we choose the Compton frequency defined by $\hbar\Omega_c = m_e c^2$, where m_e is the electron mass. This choice for the cutoff has been shown to yield correct results for other electron-ZPF interactions, for example in calculations of the Lamb shift[19, 20]. Substitution into (11) then yields an expression for the diameter d of the spherical-shell distribution,

$$d = 2a = 2(3\pi\alpha)^{1/4} \sqrt{N} \left(\frac{\hbar}{m_e c}\right) \approx \sqrt{N} \left(\frac{\hbar}{m_e c}\right). \tag{12}$$

We see that the diameter for the spherical-shell distribution predicted by this calculation is simply the Compton wavelength $\hbar/m_e c$, multiplied by the square root of the number of electrons on the shell.[2]

As with the two-particle van der Waals interaction, we need to determine whether the Schrödinger pressure plays a significant role in this configuration. The complete expression for the Schrödinger pressure exerted by N free electrons confined to volume V in their lowest energy state (N/2 with spin up, N/2 with spin down) is[17]:

$$P_S = \frac{1}{5}\left(3\pi^2\right)^{2/3} \frac{\hbar^2}{m_e}\left(\frac{N}{V}\right)^{5/3} \quad . \tag{13}$$

A direct comparison of the magnitude of the Schrödinger pressure against the vacuum and coulomb pressures, given by $(1/3)u_V$ and u_e, respectively, indicates that the Schrödinger pressure can be neglected for electron numbers of interest here, say $N \gg 10^4$.

Finally, we note that the spherical-shell configuration envisioned here satisfies the stability condition that a slight change in radius results in a restoring force that tends to return the sphere to its original size.

V. Casimir's Shell Model II

In Casimir's shell model of the second type, in place of the shielding of the interior from all ZPF fields below the Compton frequency, interior fields associated with those discrete states permitted by boundary conditions are assumed to exist, as in the parallel-plates example.

---

[2] In passing we note that this corresponds to each electron on the shell occupying a circular area with radius approximately equal to the Compton wavelength in an apparent quantum equivalent of close-packing.

One of the first models of this type to be published in the literature considered a semiclassical electron as a conducting spherical shell carrying a homogeneously-distributed surface charge e, whose tendency to expand by coulomb repulsion is checked by inwardly-directed ZPF radiation pressure (the Casimir force)[21]. Unfortunately for the model, a detailed analysis found that for this case the Casimir pressure was outwardly-directed, augmenting rather than canceling the coulomb pressure. This type of analysis was then extended to the case of solid dielectric and conducting balls[22]. For these examples the Casimir pressure turned out to be inward as required, but the analysis was still unsatisfactory with regard to certain mathematical divergences and the prediction of an erroneous value for the fine-structure constant.

Of relevance to our interests here, however, is the Casimir-effect solution for a conducting *cylindrical* shell, one of the limited number of geometries for which, fortunately, a solution is available[23]. The reason for this geometry being of interest is the observed tendency for high-density charge distributions to take the form of cylindrical filaments or, in some instances, cylinders wrapped head-to-tail to form toroids.[3] The cylindrical solution yields for the Casimir energy per unit length

$$\frac{E_{cas}}{L} = -\frac{\pi C_1 \hbar c}{a^2} \quad , \tag{14}$$

where a and L are the radius and length of the cylinder; $C_1 = 4.32 \times 10^{-3}$ is a scale factor deriving from detailed analysis of the ZPF field distribution as it matches the boundary conditions imposed by the cylindrical geometry. The associated Casimir pressure (force per unit area), $\left(F_{cas}/A\right) \rightarrow -\left(dE_{cas}/dV\right)$, is in turn given by

[3]The generation of high-charge-density entities by field emission tips have been reported to favor "smoke-ring" geometries, i.e., toroids[3].

$$\frac{F_{cas}}{A} = -\frac{C_1 \hbar c}{a^4} \tag{15}$$

The corresponding expression for the coulomb pressure is:

$$\frac{F_{coul}}{A} = \frac{(Q/L)^2}{8\pi^2 \varepsilon_0 a^2} \tag{16}$$

where (Q/L) is the charge per unit length.

Finally, the Schrödinger pressure given by (13) is found to play a significant role in the filamentary geometry, with its corresponding expression for the cylindrical geometry given by

$$\frac{F_s}{A} = \frac{3^{2/3}}{5\pi^{1/3}} \frac{\hbar^2}{m_e} \frac{1}{a^{10/3}} \left(\frac{N}{L}\right)^{5/3}, \tag{17}$$

where N is the number of charges (electrons) involved, determined by $Q = Ne$.

With the coulomb pressure proportional to $1/a^2$ and the Casimir pressure proportional to $1/a^4$, a diffuse distribution of free charge will simply disperse as the result of coulomb repulsion forces. However, if a cylindrical-shell (straw) filament of electrons reaches a critical threshold density determined by $|F_{cas}/A| \geq |F_{coul}/A|$, or

$$a \leq \frac{\sqrt{2\pi C_1/\alpha}}{(N/L)}, \tag{18}$$

then charge-filament collapse will set in (again, α is the fine structure constant). A quick calculation shows that, for example, 10^4 electrons organized into a 1-μm diameter filament, 2.5-mm long, would satisfy the condition for filament collapse, while an inch-long filament of this diameter could support 10^5 electrons.

In this model once filament collapse sets in, the $1/a^4$ Casimir pressure overwhelms the $1/a^2$ coulomb pressure, driving the filament diameter to ever-decreasing values and thus higher charge densities. Aside from classical instabilities that are certain to occur, at a formal level a limiting minimum filament diameter is predicted as quantum features emerge, specifically as represented by the Schrödinger pressure. As filament collapse occurs, the coulomb pressure becomes negligible compared to the Casimir pressure, and can therefore be neglected. The Casimir pressure with its $1/a^4$ dependence, if left unchecked, could in principle overwhelm even the Schrödinger pressure with its $1/a^{10/3}$ dependence. However, the $1/a^4$ -dependent Casimir equation, taking into account as it does retardation effects in the electromagnetic field, reverts to a $1/a^3$ van der Waals-type dependence associated with the nonretarded-field solution when separation distances become comparable to the shortest wavelength that can be reflected by the charges constituting the Casimir boundaries[24] (in this case the Compton wavelength of the electrons, as noted earlier); thus the Schrödinger pressure can become effective in preventing further collapse. This transition from a retarded to a nonretarded-solution law can be seen in the experimental data of Israelachvili and Tabor, obtained in experiments involving crossed cylinders of mica as Casimir boundaries[25].

An attempt to go further in applying detailed calculations of the above type to plasma-arc filament formation under complex laboratory conditions is surely not warranted at this point; detailed experimentation specifically to test the van der Waals/Casimir hypothesis will be required. Nonetheless, the theoretical considerations presented here indicate that van der Waals/Casimir-

type effects may well play a role in the generation of robust, high-charge-density effects that have been reported in arc-discharge experimentation.

VI. Conclusions

Laboratory observation of high-density filamentation or clustering of electronic charge has motivated an investigation into potential cohesive mechanisms whereby repulsive coulomb forces could be overcome by some form of compensatory attractive force. Of the various possibilities discussed in the literature, we have chosen to examine a class of models suggested by Casimir that invokes the possibility of charge confinement by van der Waals/Casimir-type forces. The resulting analysis indicates that although confinement of small numbers of electrons by the van der Waals mechanism cannot be achieved under realistic conditions, the cooperative action of large numbers of charges by Casimir-type effects does provide a potential candidate for charge confinement of roughly the right order of magnitude to correlate with reported laboratory observation.

Acknowledgements

This work was sponsored by the Air Force Office of Scientific Research, Bolling AFB DC.

References

1. V. Nardi, W. H. Bostick, J. Feugeas, and W. Prior, Phys. Rev. A **22**, 2211 (1980).

2. G. A. Mesyats and D. I. Proskurovsky, *Pulsed Electrical Discharge in Vacuum* (Springer-Verlag, New York, 1989).

3. K. R. Shoulders, *Method and Apparatus for Production and Manipulation of High Density Charge* (U.S. Patent 5,054,046, Oct. 1, 1991).

4. H. Fox and P. G. Bailey, Proc. 32nd IECEC (Intersociety Energy Conversion Engineering Conference), Honolulu, 1997 (preprint)

5. R. W. Ziolkowski and M. K. Tippett, Phys. Rev. A **43**, (1991) 3066.

6. H. B. G. Casimir, Proc. Kon. Ned. Akad. Wetenschap. **51**, (1948) 793.

7. M. Fierz, Helv. Phys. Acta **33**, (1960) 855.

8. T. W. Marshall, Nuovo Cimento **38**, (1965) 206.

9. T. H. Boyer, Ann. Phys. (N.Y.) **56**, (1970) 474.

10. S. K. Lamoreaux, Phys. Rev. Lett. **78**, (1997) 5.

11. P. W. Milonni, R. J. Cook, and M. E. Goggin, Phys. Rev. A **38**, (1988) 1621.

12. H. B. G. Casimir, Physica **19**, (1953) 846.

13. T. H. Boyer, Phys. Rev A **7**, (1973) 1832.

14. M. J. Renne, Physica **53**, (1971) 193.

15. H. B. G. Casimir and D. Polder, Phys. Rev. **73**, (1948) 360.

16. L. Spruch, in *Long-Range Casimir Forces: Theory and Recent Experiments on Atomic Systems*, edited by F. S. Levin and D. A. Micha (Plenum, New York, 1993).

17. V. F. Weisskopf, Science **187**, (1975) 605. See also Am. J. Phys. **53**, (1985) 109, 206, 304.

18. H. E. Puthoff, Phys. Rev. A **40**, 4857 (1989); Errata and Comments, Phys. Rev. A **44**, (1991) 3382, 3385.

19. H. A. Bethe, Phys. Rev. **72**, (1947) 339.

20. T. A. Welton, Phys. Rev. **74**, (1948) 1157.

21. T. H. Boyer, Phys. Rev. **174**, (1968) 1764.

22. K. A. Milton, Ann. Phys. **127**, (1980) 49.

23. L. L. DeRaad, Jr. and K. A. Milton, Ann. Phys. **136**, (1981) 229.

24. See, for example, E. M. Lifshitz, Sov. Phys. JETP **2**, (1956) 73.

25. J. N. Israelachvili and D. Tabor, Proc. Roy. Soc. A **331**, (1972) 19.

Temporal behavior of multiple-electron emission in single field-emission events

M. A. Piestrup[a)]

Adelphi Technology, Inc. 2181 Park Blvd., Palo Alto, California 94306

P. J. Ebert[b)]

NOLASCO - Science Consultants, 1748 Applewood Road, Baton Rouge, Louisiana 70808

(Received:

We have studied the harmonic content of current generated by a single-point bent tungsten wire in order to clarify point of origin of the emission. Previous research by us comparing thermal and field emission spatial distribution and their random emssion from the same bent wire field emitter show both to be emitted from the same emitter. Measurements of the time evolution of the harmonic content show that there are both long and short term changes in the count rate. Contamination of the field emission surface by absorption of gas molecules in the vacuum is suggested as the origin of the multiple-electron emission.

Key Words: field emission, multiple-electron emission, thermal emission

PACS: 07.77.K; 79.70+q; 85.45B

[a)] e-mail: melpie@ix.netcom.com

[b)] e-mail: pjebert@premier.net

Previously, we measured thermal and field electron emission from a modified electron-microscope W source with an energy-dispersive counting system.[1,2] Thermal-emission spectra were consistent with random emission of single electrons, while field-emission spectra were consistent with multiple-electron emission in random events. As many as 11 electrons were detected in single random-emission events in isolated random field-emission events. We compared the electron beam spot sizes of thermally-emitted electrons with that of the field-emitted electrons from the same single-point bent-tungsten wire and found them to be identical, thus demonstrating that the electrons are from the same emitter and that the harmonic content of the field emission is from the bent-tungsten wire.

Other researchers have obtained conflicting results as to the origin of this multiple emission. Hermmann and the Gazier demonstrate the multiple-emission.[3,4] Fursei et als and others have carried out numerous experiments to measure field emission statistics under a variety of experimental conditions, and have published extensively on this subject since 1975.[5-16] Their first results showed multiple emission from W and Si.[3] However, in an experiment to measure multiple emission of electrons from various facets of a clean W single crystal, only single electron emission was observed. Fursei attributed earlier results to "parasitic secondary electron

emission from the intermediate electrodes." [3] A summary of experimental results is tabulated in ref. 1.

In order to further explore the origin of this unusual electron emission behavior we have undertaken new experiments to determine the behavior of the multiple-electron field emission over time. We did this in the hope of determining possible variables that might be affecting the multiple-emission.

As in our previous work we utilized a modified Siemens Elmiskop II transmission electron microscope.[1] The electron source was standard, a commercially available W point filament that could be heated to 2800 °K. Thus, the source could be either one of thermal emission (TE) or FE. The tip was positioned in the high field acceleration region of the microscope, through the cathode's aperture. There were no intermediate electrodes between the tip and the anode, which was held at ground potential. All beam optical components such as apertures and magnetic lenses were down-stream of the anode. To center the beam on the axis of the microscope, the tip could be shifted in relation to the anode in two normal directions without breaking vacuum. The microscope, operated at 50 kV, was evacuated with an oil diffusion pump. Typical operating pressure was 5 x 10^{-5} Torr or below. The microscope column had to be extended to accommodate a 25 mm^2 Si surface barrier detector that could be translated 100 mm along a horizontal axis. The detector was 595 mm from the tip,

and was collimated with a 1-mm diameter iris to reduce the active detection area and to improve spatial resolution. The dimensions of the electron beam were controlled with the magnetic lens, and could be viewed with a retractable phosphorescent screen located 25 cm upstream of the detector. Charge pulses from the detector were processed in a counting system consisting of a preamplifier, a main amplifier, a multichannel analyzer and a count rate meter. Amplified pulses ~1μsec) were also monitored with an oscilloscope.

A Nuclear Instruments multi-channel scalar (MCS) was utilized to determine the change in harmonic content of the field emitter as a function of time. We looked at both short term ($t < 300$sec) and long term response ($\Delta t \approx 1$ hour) of the FE. A number of experiments were done using the several different field emitters at several different temperatures and vacuums. Results show that the age of the field emitter, its vacuum, and its possible poisoning by gas absorption determine the field-emission rates.

In the data shown in the following figures, we utilized a new field emitter. The field emission was first observed using our standard pulse height analysis (PHA) setup, and a PHA electron-energy spectrum was taken. The results shown in Fig. 1 again show harmonic content out to the 10th harmonic.

The pulse-height-analysis (PHA) board was set in the multi-channel scalar (MCS) mode with the dwell time set for 1 sec. In the MCS mode,

the count rate could be measured and recorded as a function of time. The discriminator of the PHA board was then set above the fundamental; thus the MCS was only counting events with multiple electrons in each event. The MCS was done immediately after the PHA spectrum of Fig. 1 was taken. Thus the field emitter had been used for over an hour. As can be seen from the Fig. 2, there was a long term decay from 600 counts/sec to 400 counts/sec. Approximately three hours later, the MCS was again taken and the rate had become an average constant rate of 127 counts/sec.

The field emission rate was observed after what we determined was the deliberate poisoning of the field emitter by heating the filament to thermal emission temperatures in a poor vacuum (6×10^{-6} Torr). The filament temperature was then reduced and the count rate measured as a function of time. The field emission harmonic content rate was found to be high but decaying rapidly. For the particular example shown in Fig. 3, the rate drops from approximately 1000 counts/sec to 100 counts/sec in approximately 180 sec, finally reaching a low, constant rate of 20 counts/sec after about 300 sec. The field emitter used here had been used for many hours and had a lower constant rate than the one used in Figs. 1-3 and did not exhibit the long term behavior of these Figs.

A heated field emitter (one whose temperature is below thermal emission temperatures) also showed similar harmonic rate changes for both long and short terms. The ratio of multiple counts to single counts as a

function of filament voltage was taken previously.[1] The harmonic content was found to drop as the filament voltage was increased. The thermal emission overwhelmed the counting system when more than 1.1 V was applied to the filament. An example of this measurement is shown in Fig. 4. The same field emitter used in Fig. 3 was used. Two interesting effects are observed when comparing Fig. 3 and 4. First, the event rate is higher (but not the harmonic content), and, secondly, the average deviation of the rate is smaller for thermalized FE. The latter becomes more apparent when we compare Fig. 3 and 4. Control over the harmonic content of FE may be important for applications of FE.

In conclusion, measurements of the time evolution of the harmonic content show that there are both long and short term changes in the count rate. Contamination of the field emission surface by absorption of gas molecules in the poor vacuum results, in increased field emission. This partially reflected in Fursei's results which saw multiple-electron emission disappear with higher quality vacuums.

This research was sponsored by the United States Air Force Office of Scientific Research, Bolling AFB DC.

1. M. A. Piestrup, H. E. Puthoff and P. J. Ebert, J. Appl. Phys. 82, 5862 (1997).

2. M. A. Piestrup, H. E. Puthoff and P. J. Ebert, "Correlated Emission of Electrons" scheduled for publication, Galilean Electrodynamics, May/June 1998.

3. M. Hermman, Z. Phys., **184**, 354 (1965).

4. C. Gazier, Phys. Lett. **35A**, 243 (1971).

5. G. N. Fursei, M. M. Mokhasne, N. V. Egorov, V. S. Ponomarev, and V. N.Shcheme-lev, Sov. Phys. Solid State **18**, 368 (1976).

6. M. M. Mokhasne, V. S. Ponomarev, N. V. Egorov, G. N. Fursei, and V. N. Shcheme-lev, Instrum. Exp. Tech. (USA) **19**, 496 (1976).

7. G. N. Fursei, N. V. Egorov and A. V. Kocheryzhenkov, Sov. Tech. Phys. Lett. 7, 343 (1981).

8. N. P. Afanas'eva, N. V. Egorov, A. V. Kocheryzhenkov and G. N. Fursei, Inst. Exp. Tech. (USA) **25**, 1204 (1982).

9. A. V. Kocheryzhenkov, V. I. Maslov and G. N. Fursei, Sov. Phys. Solid State **29**, 1421 (1987).

10. V. I. Maslov, G. N. Fursei, A. V. Kocheryzhenkov, and N. P. Afanas'eva, Instrum. Exp. Tech. (USA) **30**, 1162 (1987).

11. G. N. Fursei, A. V. Kocheryzhenkov, V. I. Maslov and A. P. Smirnov, Sov. Tech. Phys. Lett. **14**, 804 (1989).

12. V. I. Maslov, G. N. Fursei and A. V. Kocheryzhrnkov, Sov. Phys.Tech. Phys. **34**, 1192 (1989).

12. V. I. Maslov, G. N. Fursey and A. V. Kocheryzhenkov, J. de Physique **50** C8 supplement, C8-113 (1989).

13. G. N. Fursei, A. V. Kocheryzhenkov, V. I. Maslov, A. L. Shmaev and L. N. Borisov, Instrum. Exp. Tech. (USA) **33**, 152 (1990).

14. V. I. Maslov, G. N. Fursei and A. V. Kocheryzhenkov, Instrum. Exp. Tech. (USA) **33**, 395 (1990).

15. G. N. Fursey, A. V. Kocheryzhenkov and V. I. Maslov, Surface Science **246**,365 (1991).

16. F. James, P. Ebert, T. Miller, K. Wansley and T. Terry, Bull. Am. Phys. Soc. **38**, (Nov. 4-6, 1993).

17. F. James, Bull. Am. Phys. Soc. **40**, 952 (1995).

Figures:

Fig. 1. Pulse Height Analysis spectrum of a W field emitter at room temperature.

Fig. 2. The number of counts/sec of multiple-electron emission in single field-emission events as a function of time. This data was taken in the first hour of the field emitter life

Fig. 3. Short term time response of a field emitter. The cathode was first heated to thermal emission temperatures. The filament temperature was then reduced and the count rate measured as a function of time. Rate is seen to dramatically drop from 1000 counts/sec to 100 counts/sec in approximately 175 sec.

Fig. 4. Short term time response of a field emitter that has been heated (cathode voltage is 0.8 VDC) but emission is not thermal. The cathode was first heated to thermal emission temperatures (1.6 VDC). The filament temperature was then reduced to 0.8 VDC and the count rate measured as a function of time. Rate is seen to dramatically drop from 7000 counts/sec to 700 counts/sec in approximately 170 sec.

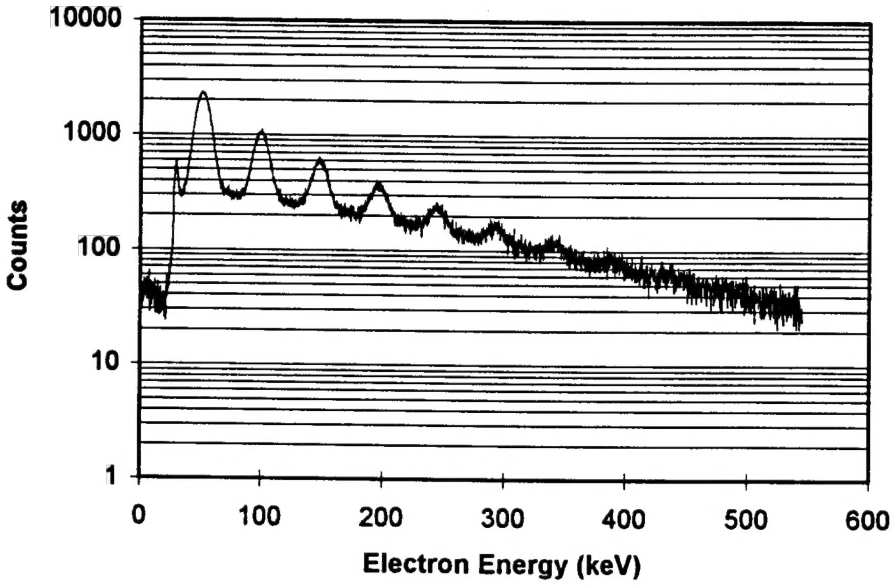

Fig. 1. Piestrup

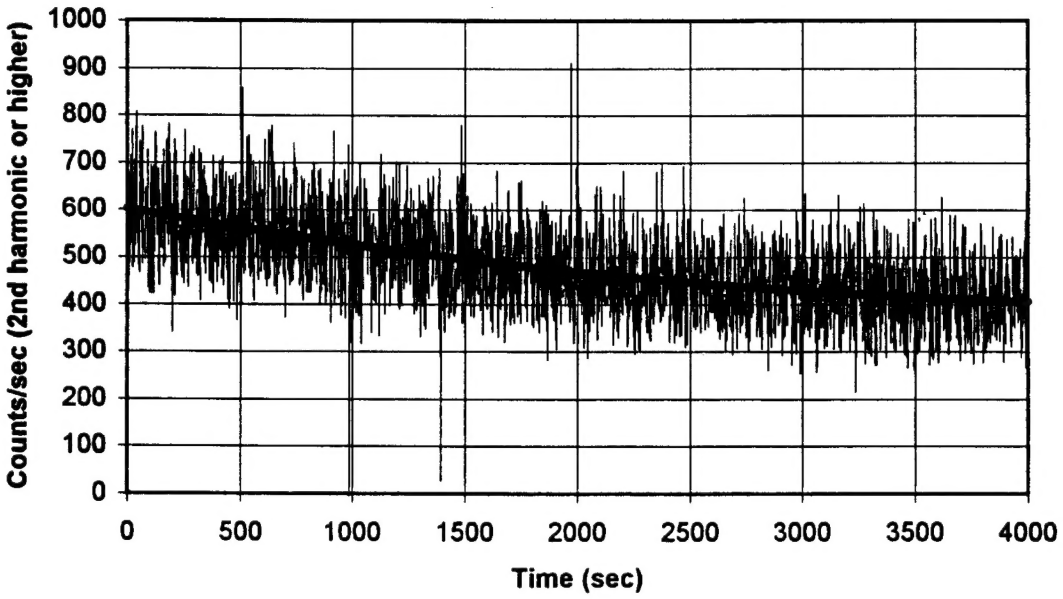

Fig. 2, Piestrup

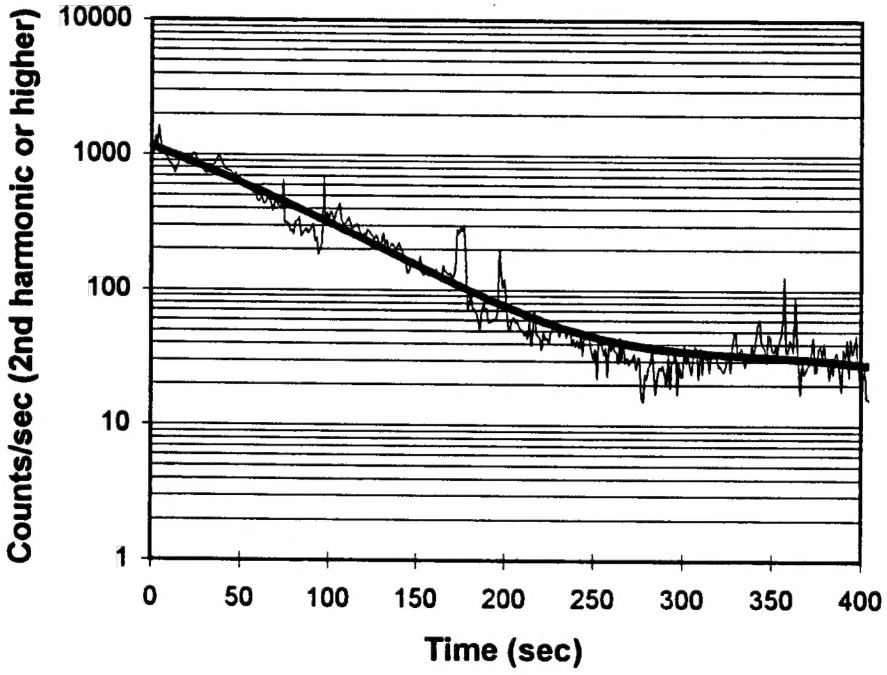

Fig. 3. Piestrup

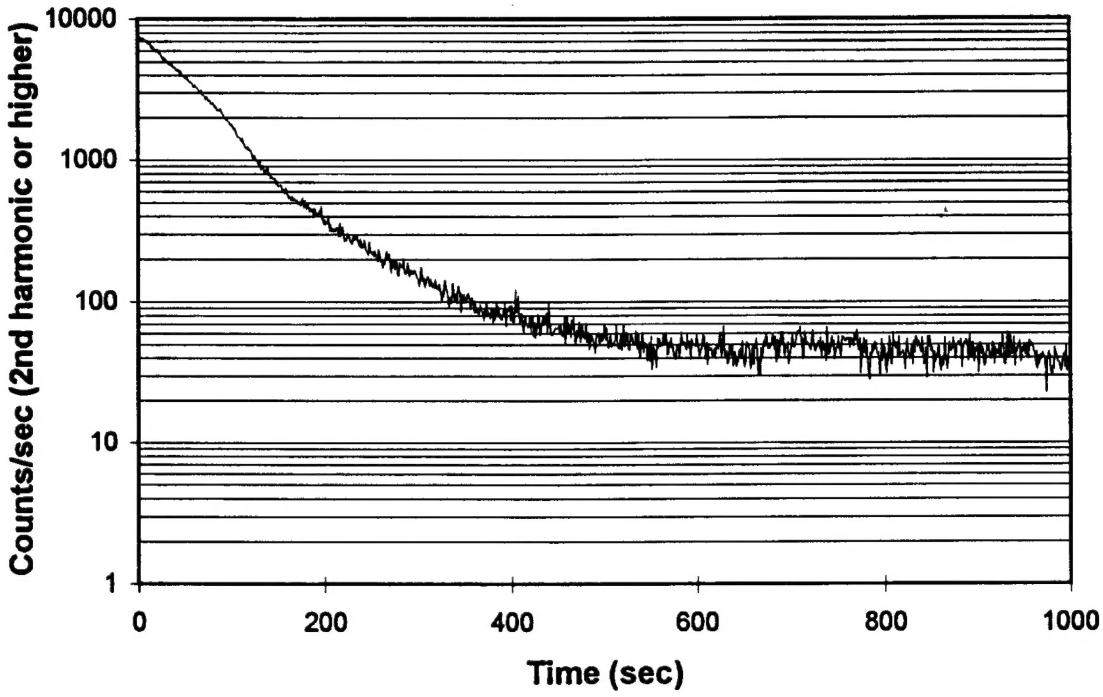

Fig. 4. Piestrup